*Digital Comprehensive Summaries of Uppsala Dissertations*
*from the Faculty of Science and Technology 2291*

# Shining Light on Benzothiadiazoles and Indolines

## *Photophysical Properties and Cancer Cell Imaging*

SUSANNE DOLOCZKI



ACTA UNIVERSITATIS
UPSALIENSIS
2023

ISSN 1651-6214
ISBN 978-91-513-1862-2
urn:nbn:se:uu:diva-508762

UPPSALA
UNIVERSITET

Dissertation presented at Uppsala University to be publicly examined in A1:111a, BMC, Husargatan 3, Uppsala, Friday, 22 September 2023 at 13:15 for the degree of Doctor of Philosophy. The examination will be conducted in English. Faculty examiner: Dr. Andrey Klymchenko (University of Strasbourg).

**Abstract**

Doloczki, S. 2023. Shining Light on Benzothiadiazoles and Indolines. Photophysical Properties and Cancer Cell Imaging. *Digital Comprehensive Summaries of Uppsala Dissertations from the Faculty of Science and Technology* 2291. 78 pp. Uppsala: Acta Universitatis Upsaliensis. ISBN 978-91-513-1862-2.

Fluorescent molecules, also called fluorophores, play an important role in life sciences. As crucial tools in fluorescence microscopy, they can be used to study biological processes on a cellular level, which is a fundamental aspect of cancer research. Depending on the specific research question, the requirements for fluorophores can be very diverse. Expanding the toolbox of fluorescent probes can therefore contribute to the possibilities of fluorescence imaging in general, especially since no single fluorophore is perfect for all applications.

In this thesis, donor-acceptor fluorophores based on two different core structures, 2,1,3-benzothiadiazole and indoline, were investigated. The compounds were photophysically studied by steady-state absorption and fluorescence spectroscopy and examined in fluorescence cell microscopy.

Monosubstituted benzothiadiazole derivatives with nitrogen-based substituents were synthesized and photophysically studied in various solvents. Fluorescence microscopy experiments revealed three promising new compounds that specifically stain lipid droplets in cancer cells. Lipid droplets are interesting cellular targets for imaging because of their high relevance in the energy metabolism of cancer cells.

Furthermore, two fluorescent indoline derivatives, which differ only by one functional group (imine vs ketone) were compared for their photophysical properties and cell imaging behavior. The indolin-3-imine derivative showed pH sensitivity due to protonation of the imine moiety, which was significantly enhanced in the excited state because of photobasicity. Fluorescence microscopy experiments showed ubiquitous cell staining with a tendency towards lysosomes, which are acidic cell organelles. In contrast, the indolin-3-one analogue featured lipid droplet-specific staining, although with rapid photobleaching. Spectroscopic studies in solution revealed photoisomerization through ring-opening upon irradiation, which explained the emission bleaching during microscopy. While this behavior is not beneficial for imaging applications, it was found that the indolin-3-one exhibited photoactivated cytotoxicity, which likely arises from singlet oxygen generation.

*Susanne Doloczki, Department of Chemistry - BMC, Organic Chemistry, Box 576, Uppsala University, SE-75123 Uppsala, Sweden.*



ISSN 1651-6214
ISBN 978-91-513-1862-2
URN urn:nbn:se:uu:diva-508762 (http://urn.kb.se/resolve?urn=urn:nbn:se:uu:diva-508762)

# List of Papers

This thesis is based on the following Papers, which are referred to in the text by their Roman numerals.

I. **Doloczki, S.**; Holmberg, K. O.; Fdez. Galván, I.; Swartling, F. J.; Dyrager, C. Photophysical characterization and fluorescence cell imaging applications of 4-*N*-substituted benzothiadiazoles. *RSC Adv.* **2022**, *12* (23), 14544–14550.

II. **Doloczki, S.**; Kern, C.; Holmberg, K. O.; Zhao, M.; Swartling, F. J.; Streuff, J.; Dyrager, C. An Indolin-3-imine Photobase and pH Sensitive Fluorophore. *Submitted manuscript*.

III. **Doloczki, S.**; Kern, C.; Holmberg, K. O.; Swartling, F. J.; Streuff, J.; Dyrager, C. Photoinduced Ring-Opening and Phototoxicity of an Indolin-3-one Derivative. *Chem. Eur. J.* **2023**, e202300864.

The following publications are not included as part of this thesis:

IV. Colas, K.;‡ **Doloczki, S.**;‡ Kesidou, A.; Sainero-Alcolado, L.; Rodriguez-Garcia, A.; Arsenian-Henriksson, M.; Dyrager, C. Photophysical Characteristics of Polarity-Sensitive and Lipid Droplet-Specific Phenylbenzothiadiazoles. *ChemPhotoChem* **2021**, *5* (7), 632–643.

V. Colas, K.; Holmberg, K. O.; Chiang, L.; **Doloczki, S.**; Swartling, F. J.; Dyrager, C. Indolylbenzothiadiazoles as highly tunable fluorophores for imaging lipid droplet accumulation in astrocytes and glioblastoma cells. *RSC Adv.* **2021**, *11* (39), 23960–23967.

VI. Colas, K.; **Doloczki, S.**; Posada Urrutia, M.; Dyrager, C. Prevalent Bioimaging Scaffolds: Synthesis, Photophysical Properties and Applications. *Eur. J. Org. Chem.* **2021**, *2021* (15), 2133–2144.

‡ These authors contributed equally.

# Disclosure of underlying licentiate thesis and the author's contributions to Papers I–III

Chapters 1.1, 1.4, and 3 of this doctoral thesis are based on the author's licentiate thesis entitled *Development of fluorescent probes based on the benzothiadiazole scaffold*, which was presented on 20th May 2021.

| | |
|---|---|
| Paper I | Performed experimental work (including synthesis, photophysical measurements, logP determination, cell staining, immunofluorescence colocalization, and fluorescence microscopy), computations, data analysis, and interpretation of results. Wrote the first manuscript draft including supporting information and contributed to their finalization. |
| Paper II | Performed photophysical measurements, NMR spectroscopy experiments, cell staining and colocalization, fluorescence microscopy, computations, data analysis, and interpretation of results. Wrote the first manuscript draft including supporting information and contributed to their finalization. |
| Paper III | Performed the methylation of the studied compound, photophysical measurements, NMR spectroscopy experiments, cell staining and colocalization, fluorescence microscopy, irradiation experiments, data analysis, and interpretation of results. Wrote the first manuscript draft including supporting information and contributed to their finalization. |

For Papers I–III, K. O. Holmberg or M. Zhao were responsible for the cell cultures, preparing cells for experiments, and performing cell viability assays.

# Contents

# Abbreviations

| | |
|---|---|
| $\varepsilon$ | Molar extinction coefficient |
| $\Phi_F$ | Fluorescence quantum yield |
| $\lambda_{Amax}$ | Wavelength of maximum absorption |
| $\lambda_{em}$ | Detected emission wavelength |
| $\lambda_{Emax}$ | Wavelength of maximum emission |
| $\lambda_{ex}$ | Excitation wavelength |
| *Abs* | Absorbance |
| aq. | Aqueous |
| BODIPY | Boron dipyrromethene |
| BTD | 2,1,3-Benzothiadiazole |
| Compd. | Compound |
| D-A | Donor-acceptor |
| dba | Dibenzylideneacetone |
| DFT | Density functional theory |
| DMSO | Dimethyl sulfoxide |
| EDG | Electron-donating group |
| ESPT | Excited state proton transfer |
| $E_T(30)$ | Reichardt's solvent polarity parameter |
| EtOH | Ethanol |
| EWG | Electron-withdrawing group |
| HAT | Hydrogen atom transfer |
| HDF | Human dermal fibroblasts |
| IC | Internal conversion |
| ICT | Intramolecular charge transfer |
| *i*-PrOH | *iso*-Propanol |
| ISC | Intersystem crossing |
| LD | Lipid droplet |
| LE | Locally excited |
| logP | Logarithmic octanol-water partition coefficient |
| MDA-MB-231 | Human breast cancer cell line |
| MeCN | Acetonitrile |
| MeOH | Methanol |
| NMR | Nuclear magnetic resonance |
| PEPPSI-IPr | [1,3-Bis(2,6-diisopropylphenyl)imidazol-2-ylidene](3-chloropyridyl)-palladium(II) dichloride |

| | |
|---|---|
| Ph | Phenyl |
| pH | Negative logarithm of hydrogen ion concentration |
| p$K_a$ | Negative logarithm of acid dissociation constant |
| p$K_a^*$ | Excited state p$K_a$ |
| RuPhos | 2-Dicyclohexylphosphino-2′,6′-diisopropoxybiphenyl |
| SK-MEL-28 | Human melanoma (skin cancer) cell line |
| $S_n$ | Electronic singlet state (n = 0 ground state, n = 1 first excited state, n = 2 second excited state) |
| $T_1$ | First electronically excited triplet state |
| THF | Tetrahydrofuran |
| UV-vis | Ultraviolet-visible |
| v | Vibrational state |
| VR | Vibrational relaxation |

# 1 Introduction

Fluorescent compounds, also called fluorophores, are important tools for a variety of applications in material and life sciences. For instance, they are used in fluorescence microscopy for bioimaging, which comprises biological samples such as animals, tissues, and cells. Fluorescence microscopy has emerged as an indispensable technique to study biological processes on a cellular level. Fluorophores are hereby utilized to target and image cell organelles or biomolecules of interest to investigate altered processes associated with diseases, such as cancer. Cancer is a complex class of diseases and represents one of the main causes of premature death worldwide.[1] Fluorescence microscopy holds promise as a non-invasive diagnostic tool and a couple of fluorescent dyes are in clinical use for image-guided tumor surgery.[2] Irrespective of its intended application, fluorescence imaging is a method that strongly depends on the availability of suitable fluorescent compounds. Hence, the development of fluorophores with improved properties tailored to specific demands is very important within chemical biology.

In pursuit of developing fluorescent probes for cancer imaging, this thesis investigates the photophysical properties and cell imaging ability of small organic fluorophores. Paper I, discussed in Chapter 3, focuses on mono-substituted 2,1,3-benzothiadiazole (BTD) derivatives that accumulate in intracellular lipid droplets (LDs), which are organelles with a crucial role in the energy metabolism of cancer cells. Papers II and III concern two fluorescent indoline derivatives that structurally only differ by one functional group (imine vs ketone). Chapter 4 compares the photophysical properties of these two compounds and their behavior when applied to cells.

The multidisciplinary work discussed in this thesis demands a short introduction to the basics of fluorescence, fluorescence microscopy, fluorophores, and LD-targeted cell imaging (Sections 1.1–1.4).

## 1.1 Principles of fluorescence

Molecules can interact with light by absorbing photons with appropriate energy. The absorption energy is strongly dependent on the structure of the molecule, with large conjugated π-electron systems enabling absorption of

light in the visible spectrum. The absorption efficiency is characterized by the molar extinction coefficient ($\varepsilon$), which is a compound-specific constant that is wavelength-dependent and can be affected by the solvent. According to the Beer-Lambert law ($Abs = \varepsilon \cdot c \cdot l$), $\varepsilon$ is linearly proportional to the absorbance ($Abs$) in dilute solutions and can be determined by ultraviolet-visible (UV-vis) spectroscopy when sample concentration ($c$) and optical path length ($l$) are known.[3,4]

Photon absorption elevates a compound from the ground state ($S_0$) to an electronically excited singlet state ($S_n$, $n > 0$) in approximately $10^{-15}$ s, which, according to the Franck-Condon principle, is faster than nuclear motion.[4-6] The compound can relax from $S_n$ in multiple ways, which can be schematically presented using the Jablonski diagram.[4,7] Figure 1 illustrates a simplified Jablonski diagram with various electronic ($S_0$, $S_1$, $S_2$, $T_1$) and vibrational states (v) of a molecule as well as possible transitions between them.

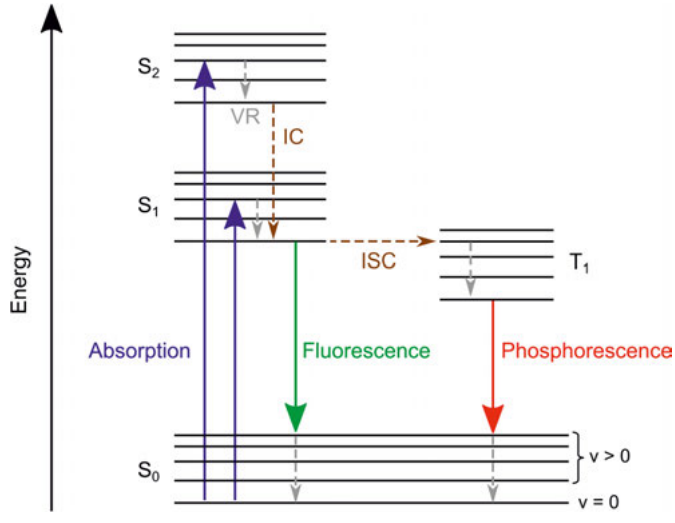


Figure 1. Simplified Jablonski diagram illustrating radiative (solid lines) and non-radiative (dashed lines) transitions initiated by photon absorption. Each electronic state ($S_0$, $S_1$, $S_2$, $T_1$) consists of various vibrational states (v) with v = 0 representing the vibrational ground state. The following non-radiative transitions are displayed: vibrational relaxation (VR), internal conversion (IC), and intersystem crossing (ISC).

Following the absorption event, the vibrational ground state of $S_n$ (v = 0) is reached by vibrational relaxation (VR) in about $10^{-12}$ s, from which several transitions can occur.[4] Non-radiative relaxation from $S_n$ to $S_{n-1}$ is called internal conversion (IC) and typically happens in the VR timescale.[4] Radiative transition through emission of a photon from $S_1$ to $S_0$ is known as fluorescence. According to Kasha's rule, this emissive process can only originate from the $S_1$ (v = 0) state.[8] Consequently, the fluorescence energy is independent of the excitation wavelength ($\lambda_{ex}$). Due to energy loss through VR, the fluorescence

maximum ($\lambda_{Emax}$) is shifted to longer wavelengths (i.e., bathochromically) as compared to the absorption maximum ($\lambda_{Amax}$) of the $S_0$-$S_1$ transition. This gap is known as Stokes shift.[4] Solvent effects can have a significant impact on $\lambda_{Amax}$ and $\lambda_{Emax}$ of a dissolved compound by stabilizing or destabilizing ground and excited states differently. The correlation between Stokes shift and solvent polarity is typically visualized by Lippert-Mataga plots.[4,9,10]

Non-radiative transition from $S_1$ (v = 0) to the triplet excited state $T_1$ (v > 0) requires spin conversion and is therefore improbable to happen. Nevertheless, this so-called intersystem crossing (ISC) can be promoted, for example, by spin-orbit coupling with heavy atoms. The subsequent radiative transition to $S_0$ is termed phosphorescence. Due to its spin-forbidden nature, phosphorescence happens on a slow timescale of typically $10^{-3}$–1 s, which is much longer than the fluorescence timescale of $10^{-8}$ s.[4]

Electronic transitions and thus spectroscopic behavior are strongly dependent on the structure of molecules. For instance, donor-acceptor (D-A) fluorophores, which combine an electron-donating group (EDG) with an electron-withdrawing group (EWG) in one molecule, often undergo intramolecular charge transfer (ICT) to form charge separated excited state species with lower energy than the locally excited (LE) state. Depending on the structure of the fluorophore and the solvent polarity, fluorescence from the LE or the ICT state can be promoted, with the latter always being red-shifted.[4,11,12]

The fluorescence quantum yield ($\Phi_F$) can simply be defined as the number of emitted photons per absorbed photon and can therefore not exceed unity.[4] Fluorescence measurements should be carried out at very low concentrations ($Abs < 0.1$) to avoid inner filter effects and self-quenching.[13] Taking this into consideration, $\Phi_F$ is often determined using the comparative method, which is based on a reference compound with known quantum yield. For the presented Papers (I–III), quinine sulfate in aqueous (aq.) $H_2SO_4$ ($\Phi_F = 0.55$)[14] or fluorescein in aq. NaOH ($\Phi_F = 0.93$)[14,15] were used as references. Emission spectra at different concentrations are measured of both, reference (ref) and compound (compd) of interest under the same conditions. The area enclosed by the emission band is integrated and the values are plotted against the absorbance at $\lambda_{ex}$. Applying a linear fitting function, the slope for the reference ($m_{ref}$) and the slope for the compound of interest ($m_{compd}$) can be determined. Finally, $\Phi_{F,compd}$ can be calculated using the following equation, which also takes the refractive indices ($n$) of the corresponding solvents into account.[4]

$$\Phi_{F,compd} = \Phi_{F,ref} \cdot \frac{m_{compd}}{m_{ref}} \cdot \frac{n_{compd}^2}{n_{ref}^2}$$

The mathematical product of $\varepsilon$ and $\Phi_F$ is called brightness and is often used in the context of fluorescence microscopy.

## 1.2 Fluorescence microscopy

Fluorescent molecules are indispensable tools in fluorescence microscopy, which is an invaluable imaging method in many life sciences. In the last decades, super-resolution techniques have been developed, with the Nobel Prize in Chemistry being dedicated to the progress in the field in 2014.[16] Nevertheless, the fluorescence microscopes most commonly found in laboratories nowadays are still the widefield and confocal fluorescence microscopes.

The basic setup of a typical fluorescence microscope consists of a light source, optical filters, a dichroic mirror, an objective, and a detector system with an eyepiece or a camera (or both).[17] As illustrated in Figure 2, the excitation filter determines the wavelength range used to excite the sample ($\lambda_{ex}$) and the dichroic mirror reflects that light to the sample while transmitting longer wavelengths (i.e., the emission of the sample) to the detector. An emission filter can be used to select the range of wavelengths that is finally detected ($\lambda_{em}$).

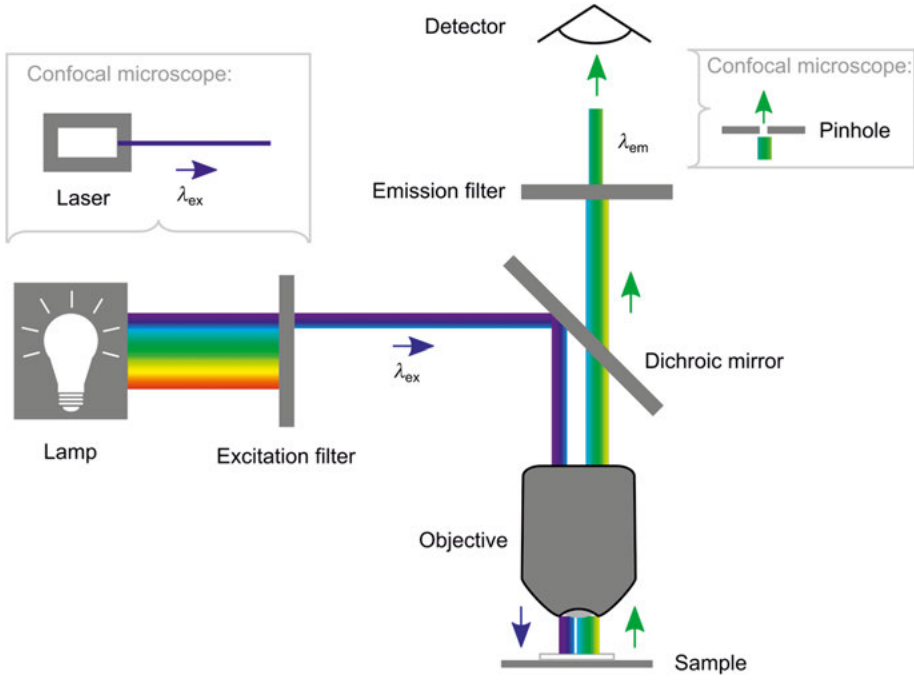


Figure 2. Simplified schematic illustration of the function principle of fluorescence microscopes. Distinctive features of typical confocal microscopes are indicated in light grey boxes.

The dichroic mirror and filters can be combined in a so-called filter cube.[17] Usually, several filter cubes are installed that allow imaging across the UV-vis light spectrum. The widefield fluorescence microscope used in this work

has, for example, a blue channel with $\lambda_{ex}$ = 325–375 nm and $\lambda_{em}$ = 435–485 nm, and a green channel with $\lambda_{ex}$ = 460–500 nm and $\lambda_{em}$ = 512–542 nm.

The essential additional component that distinguishes a confocal microscope from the widefield alternative is a pinhole in front of the detector that rejects out-of-focus light and thus allows for better resolution of the acquired image (Figure 2). Furthermore, confocal laser scanning microscopes use lasers to excite a small spot, which is scanned over the sample to construct the image.[18]

## 1.3 Prevalent fluorophores used for cell imaging

The basis of organic fluorophores is typically a (hetero)aromatic scaffold. Some of the most common structures in fluorescent dyes for bioimaging are coumarins, boron dipyrromethenes (known as BODIPY dyes), cyanines, and xanthenes (Figure 3).[19-22] Xanthenes constitute the core of fluoresceins and rhodamines. If the fluorophore itself shows adequate specificity for a cellular target, it can be applied directly to cells for staining, while unspecific fluorophores can be used as fluorescent labels, e.g., for immunofluorescence.

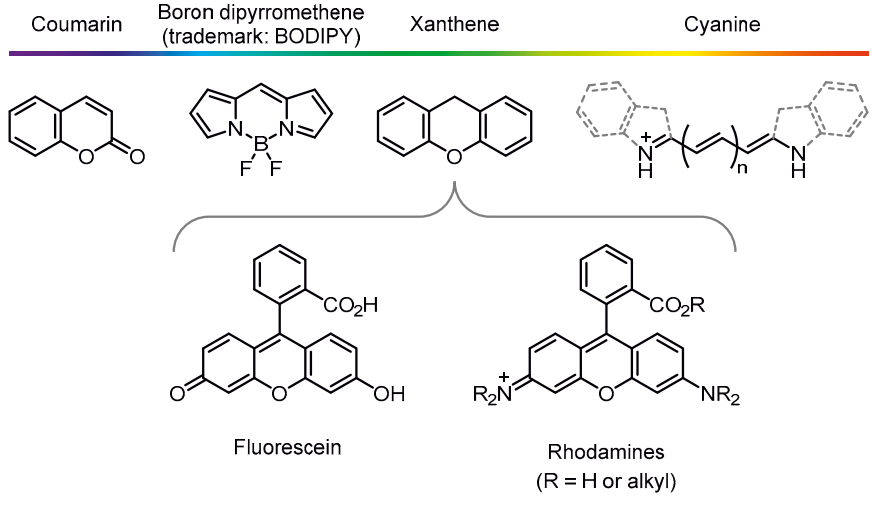


Figure 3. Common core structures of fluorescent dyes used for bioimaging. The color spectrum indicates typical spectral regions of emission of the compound classes.

Immunofluorescence is a commonly used method, in which a primary antibody is used to target a specific biomolecule in the cell.[23] Usually, a secondary antibody tagged with a fluorophore is subsequently used to bind to the primary antibody, thereby visualizing the target. Alternatively, fluorophore-labeled primary antibodies can be utilized, circumventing the need for a secondary antibody. Although this staining method is very versatile

with respect to target variety, it requires rather expensive antibodies, multi-step staining procedures, and fixation of the cells (followed by permeabilization) since antibodies typically have very poor cell permeability.[23] The latter poses a significant limitation to applications as immunofluorescence experiments cannot be performed on living cells. Nevertheless, immunofluorescence is commonly used for co-staining in the development of new organelle-targeted fluorescent probes to ascertain the probe localization.

Small molecular fluorescent probes, unless highly polar, are usually cell permeable and thus can be used for live cell imaging, provided that the cell viability is not affected. Simple and quick staining procedures can also be highlighted as an advantage. On the other hand, careful consideration should be given to the selection of a suitable fluorophore that meets the specific demands of the experiment. For example, fluoresceins[24] and long-chain cyanines[25,26] often suffer from low photostability, which is especially problematic when long-term imaging is desired. BODIPY dyes are infamous for their small Stokes shifts,[27] which may lead to low signal to background ratios due to scattering of excitation light or reabsorption effects.[28,29] Extensive efforts have been dedicated to improve the properties of fluorophores based on these established core structures, such as increasing the photostability,[29-35] the Stokes shift,[27-29,36-41] and the brightness.[29,42,43] Moreover, fluorophores with core structures beyond these classical scaffolds have been developed, such as indolizines,[44-47] $BF_2$ formazanates,[48-51] Si-rhodamines,[52-57] or BTDs.[58-61]

Derivatives of BTD are the focus of Chapter 3 of this thesis, while Chapter 4 describes the introduction of a new structure for cell imaging, namely indolin-3-imine, which is compared with the rather underexplored indolin-3-one analogue.

## 1.4 Organelle-targeted fluorescence cell imaging

Eukaryotic cells enclose various organelles with different functions that can be affected by diseases. Organelle-specific imaging is therefore important to study these diseases with respect to therapeutical approaches but also as diagnostic means.

Fluorescent probes for organelle-targeted cell imaging should ideally show high target specificity without background staining, high brightness and photostability, good cell permeability, large Stokes shift, as well as narrow absorption and emission profiles. The latter is particularly important for multicolor imaging applications (e.g., colocalization experiments). Furthermore, the fluorescent probe should not be cytotoxic or interact with its target in a way that influences its properties and function.[62,63]

As mentioned before, antibodies that selectively bind to organelle-specific proteins can be used. Alternatively, molecular fluorescent probes can be equipped with structural motifs that selectively target organelles.[64-66] For example, weakly basic amines (typically morpholine) linked to the fluorophore can be used as a targeting group for lysosomes due to the low lysosomal pH.[67,68] And cationic moieties such as triphenylphosphonium typically localize in mitochondria because of the negative mitochondrial inner membrane potential.[69,70] Moreover, LDs can be targeted using lipophilic probes.[71,72] This will be discussed in more detail in the following Sections as the majority of the presented Papers in this thesis concern LD-specific fluorophores.

### 1.4.1 Lipid droplets and their role in cancer cells

Lipid droplets (LDs) are spherically shaped organelles, consisting of a hydrophobic core (mainly triacylglycerols and cholesteryl esters) enclosed by a phospholipid monolayer (Figure 4). This membrane is decorated with diverse proteins that control several aspects of LD dynamics, such as growth, degradation and organelle interactions.[73-75]

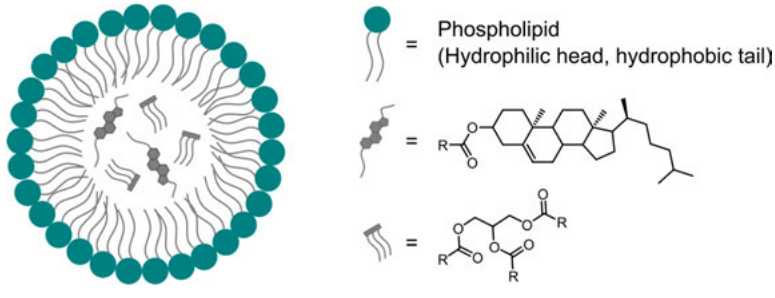


Figure 4. Simplified structure of a lipid droplet illustrating a phospholipid monolayer enclosing triacylglycerols and cholesteryl esters. R = hydrocarbon chains.

After their formation in the endoplasmic reticulum, LDs are released into the cytosol, where they mainly serve as energy storage for the cell. They are degraded via lipolysis or lipophagy to provide energy for metabolic processes or substrates for membrane synthesis during cell proliferation.[73] Nutrient deprivation initiates hydrolysis of the neutral lipids in the LD core, making fatty acids available for $\beta$-oxidation in mitochondria or peroxisomes and thus re-establishing the energy supply. An additional function of LDs is to protect the cell from lipotoxicity by capturing free fatty acids in the cell, which are considered toxic.[73,74]

Altered LD metabolism is associated with several metabolic diseases such as obesity, diabetes, cardiovascular diseases, or cancer. LDs represent

substantial elements in energy metabolism and are therefore involved in all stages of cancer development.[73-75]

Lipid droplets are obviously characteristic for adipocytes but in the last decade LD accumulation has been attributed to various types of cancer, such as breast and prostate cancers, as well as melanoma.[74,76,77] Furthermore, oxygen-deficiency (i.e., hypoxia) in cancer cells typically contributes to the accumulation of LDs. Tumor hypoxia is a result of excessive cell proliferation that outgrows the vascular supply and thus is associated with high aggressiveness and poor prognosis.[78-80] The cancer cell metabolism is reprogrammed in order to ensure survival, including increased lipogenesis and thus LD accumulation.[75] Irrespective of whether the cancer cells are hypoxic (1–5% $O_2$) or normoxic (10–21% $O_2$),[81] LD dynamics have significant impact on cancer cell proliferation and resistance to death, for example through chemotherapy. LDs can therefore serve as high potential biomarkers for cancer diagnosis and prognosis.[75]

## 1.4.2 Fluorescent probes targeting lipid droplets

Access to adequate imaging tools is the vital basis of studying LDs and their role in cellular metabolic processes. Fluorescence imaging has emerged as a highly sensitive technique that typically enables straightforward sample preparation and, in many cases, live-cell imaging. The latter is especially important when LD dynamics are to be studied. Some of the most commonly used and commercially available fluorescent probes for LDs are **Nile Red**, **BODIPY 493/503**, and **Oil Red O** (Figure 5).[82-85]

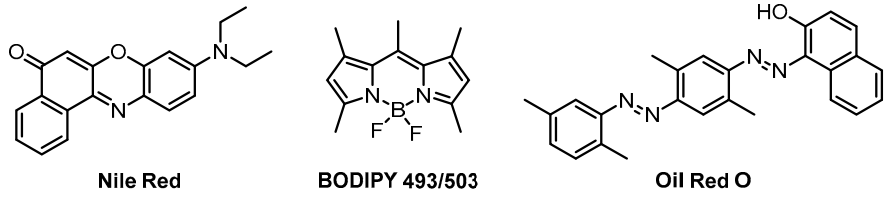


Figure 5. Commercially available fluorophores for LD staining.

The major benefit of **Oil Red O** is certainly its inexpensiveness, but its insolubility in water limits its application to fixed cells. Furthermore, the alcoholic solution needed for cell staining, can affect the lipid droplets in the cell.[86,87] **Nile Red** and **BODIPY 493/503** are often used for colocalization experiments in the development of new LD probes to confirm LD staining patterns. However, when performing imaging experiments, some unfavorable properties of these fluorescent dyes need to be taken into consideration. **Nile Red** is known for staining various lipid structures in the cell (not only LDs) and its broad absorption and emission profiles can lead to channel

overlap and therefore limit its use in multicolor fluorescence imaging.[71,83,86] **BODIPY 493/503** is more selective for LDs than **Nile Red** and its narrower absorption and emission bands are beneficial for multicolor fluorescence imaging. On the downside, the BODIPY dye is less photostable and features unfavorably small Stokes shifts.[63,71,86]

During the last decade, a variety of fluorescent probes for LDs based on small molecules have been developed. While extensive summaries of reported LD dyes have been published in a few review articles,[71,72,88] some selected examples with particular relevance for this thesis are appropriately discussed in Chapters 3 and 4.

# 2 Aims of the thesis

The overall objective of the presented work in this thesis was to contribute to the development of fluorescent probes for cell imaging based on the benzothiadiazole and indoline scaffolds (Figure 6). To accomplish this, the effect of structural modifications of the fluorophores on the photophysical properties as well as their ability to target and specifically image cellular organelles were investigated.

The work described in Chapter 3 (Paper I) aimed to synthesize a series of 4-*N*-substituted BTD derivatives (Figure 6) and to study their photophysical properties in various solvents using steady-state absorption and fluorescence spectroscopy. The aim was further to examine the utility of the compounds as probes for fluorescence cell microscopy, with focus on LD-specific imaging.

The work described in Chapter 4 aimed to investigate and compare the photophysical properties and cell imaging utility of a fluorescent indolin-3-imine derivative (Paper II) and its ketone analogue (Paper III; Figure 6), including their effect on cell viability.

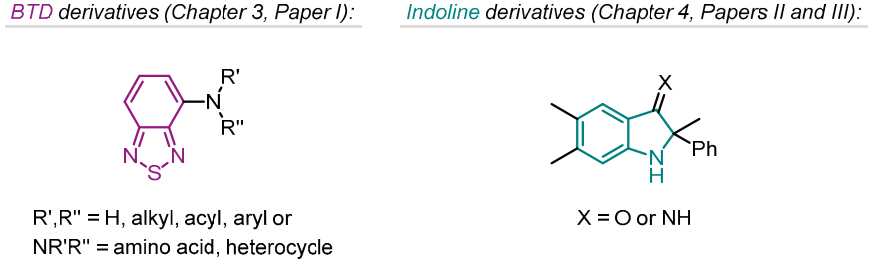


Figure 6. Overview of the fluorophores studied in this thesis. The BTD and the indoline core structure is highlighted in purple and teal, respectively.

# 3 Fluorescent benzothiadiazole derivatives for lipid droplet imaging (Paper I)

## 3.1 Background

Benzothiadiazole (BTD, Figure 7) is a heterocyclic molecule with electron-poor, aromatic character.[89] In the last decade, it has attracted remarkable attention as an electron accepting unit in organic electronics, such as organic light-emitting diodes and photovoltaic devices.[90-93] Furthermore, many BTD derivatives with electron-donating substituents have been applied as fluorescence imaging probes for cell biology.[61,94,95] BTD-based fluorophores typically unite characteristics that are favorable for bioimaging, including large Stokes shifts, high (photo)stability, and membrane permeability.[94] Two examples of BTD-based fluorophores that have shown organelle specificity in fluorescence cell imaging are depicted in Figure 7. The compound named **Splendor** was reported as a fluorescent probe for selective staining of mitochondria in cancer cells,[59] while **DBTD** was applied to selectively image lysosomes.[96] Both compounds are D-A fluorophores, generated by combining EDGs with the electron-withdrawing BTD scaffold (Figure 7). The electron acceptor strength of BTD in **Splendor** is enhanced by an electron-withdrawing 2-pyridinylethynyl substituent in *para*-position to the donor. In general, the photophysical properties of BTD-based fluorophores can be tuned quite readily by substituent modifications.

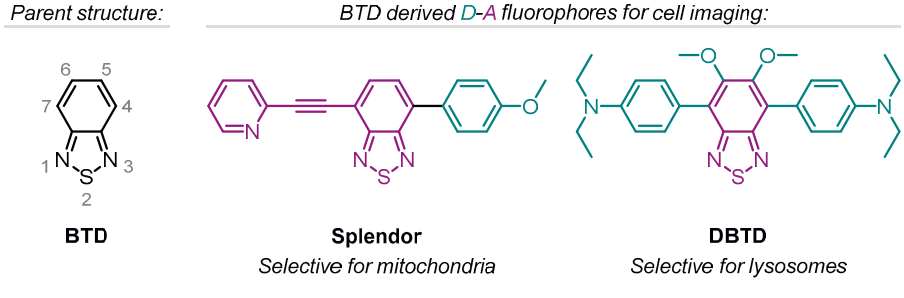


Figure 7. Structure of 2,1,3-benzothiadiazole (BTD) with atom numbers indicated in grey. **Splendor** and **DBTD** are examples of D-A fluorophores based on BTD that can be used for organelle selective cell imaging.[59,96] Donor and acceptor units are depicted in teal and purple, respectively.

The following Sections comprise further introduction to the synthesis of BTD derivatives and examples of BTD-based fluorophores used for cell imaging, with particular focus on LD-specific probes. Subsequently, the synthesis, photophysical properties and LD imaging utility of a series of fluorescent 4-*N*-substituted BTD derivatives (Paper I) is presented.

### 3.1.1 Synthesis of benzothiadiazole derivatives

The most common method to synthesize BTD is by ring-closure of 1,2-diaminobenzene with thionyl chloride in the presence of a base.[91,97] Subsequent electrophilic aromatic substitution with molecular bromine yields 4-bromo-BTD or 4,7-dibromo-BTD,[98] which are popular precursors for further versatile structural modifications such as cross-coupling reactions to generate π-extended BTD derivatives.[91] For instance, **Splendor** (Figure 7) was synthesized by successive Sonogashira and Suzuki-Miyaura couplings.[59] The BTD positions C5 and C6 are more difficult to access synthetically and substituents there are often introduced on the 1,2-diaminobenzene derivative before ring-closure with a sulfur source. This approach has, for example, been used in the synthesis of 5-bromo-BTD[98] and **DBTD**[96] (Figure 7). Good nucleophiles, such as many amines, can be introduced by simple nucleophilic aromatic substitution if the electron-poor nature of 4-halide-substituted BTD is further amplified by an EWG on C7, such as a cyano or a sulfonyl group.[99-101] If this condition is not given, palladium-catalyzed Buchwald-Hartwig aminations of brominated BTD are often the method of choice.[58,102-104] In line with a few other approaches towards the direct functionalization of BTD,[105-111] very recently, a photochemical amination protocol for BTD with secondary amines was reported.[111] Moreover, BTD can act as a directing group for Pd(II)-catalyzed reactions, including arylations and halogenations. Phenyl-BTDs[112,113] and amido-BTDs[114,115] have been further functionalized using this strategy.

The BTD core demonstrates high chemical stability under most conditions. However, reducing agents such as $LiAlH_4$[116], Mg/methanol[117] or in some cases even $NaBH_4$[118,119] cause reductive sulfur extrusion to yield 1,2-diaminobenzenes.[91] Finally, it should be noted that many BTD derivatives used as precursors in synthesis are commercially available nowadays, such as various brominated BTD derivatives and 4-amino-BTD.

### 3.1.2 Benzothiadiazole-based fluorophores for cell imaging

Many small BTD derivatives have been studied for their use in fluorescence microscopy. In this regard, B. A. D. Neto and co-workers deserve a mention due to their pioneering and continuous work to develop fluorescent BTD derivatives for bioimaging applications.[61] Besides mitochondria and lysosomes, as mentioned previously (Figure 7), BTD derivatives for specific staining of nuclei, plasma membranes, or LDs have also been reported.[61] In Figure 8, a selection of BTD-based compounds is presented, which highlights the significant impact on target selectivity that small molecular modifications can have. For example, 4-*N*-naphthylamino-BTD stains mitochondria whereas the quinoline analogue (one carbon replaced with nitrogen) stains lipid droplets (Figure 8A).[120,121] Additionally, the position of the pyridine nitrogen atom in 4-*N*-pyridylamino-BTD can affect mitochondria staining, as well as bromide substitution on C7 of BTD (Figure 8B).[122-124] Furthermore, including an acetylene linker between the two aromatic units of phenyl-BTD turns an unspecific fluorophore into a fluorescent probe for LDs (Figure 8C).[120,125]

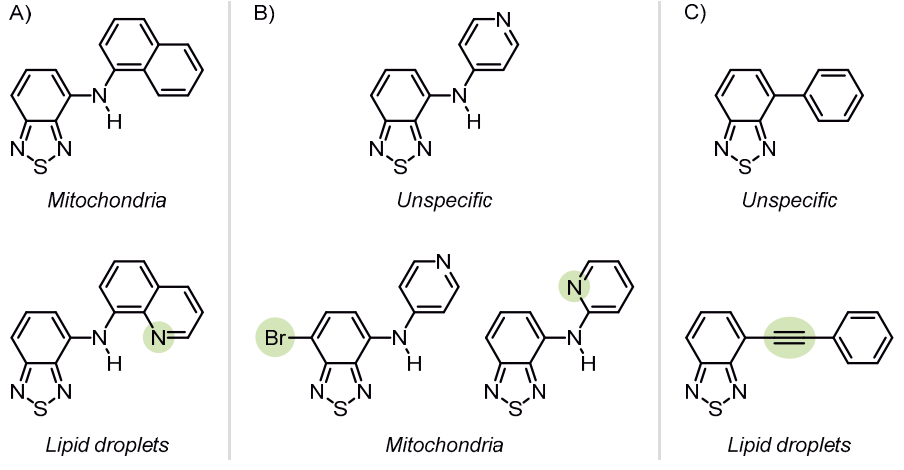


Figure 8. Selected examples[120-125] of fluorophores showing that even small molecular modifications (highlighted in green) can affect the staining pattern and organelle selectivity in cells.

The first BTD-based fluorescent probe specific for LDs was an oleamide conjugate, which was reported by Neto and co-workers in 2014 (**BTD-AO**, Figure 9).[60] The subsequent development of smaller LD-specific BTD derivatives has shown that it is not necessary to use such a highly lipophilic substituent to achieve LD staining. **BTD-QN**,[121] **BTD-CCPh**,[125] and **LD-BTD1**[126] (Figure 9) represent such small monosubstituted fluorescent probes. The compound **LD-BTD1** was reported by Dyrager and co-workers in 2017 to provide nearly background-free LD staining in melanoma cells (i.e., skin cancer cells).[126] The fluorophore showed favorable photophysical

properties for fluorescence imaging of LDs, such as large Stokes shifts, high $\Phi_F$ in apolar solvents, and fluorescence quenching in aq. environments.[126] Figure 9 shows its photophysical data in comparison with other LD-specific dyes. Its great imaging results towards LDs were ascribed to a combination of relatively high lipophilicity (experimental logP = 3.3)[126] and strong fluorescence quenching in aq. environment, such as the cytosol. On the other hand, low water solubility and a relatively low brightness (due to low $\varepsilon$) were attributed to **LD-BTD1**.

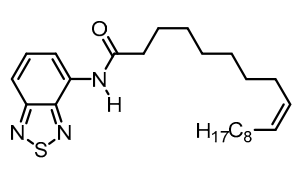

**BTD-AO**

Toluene / EtOH

$\lambda_{Amax}$ 375 / 365 $\varepsilon$ 2.7 / 2.9 × $10^3$

$\lambda_{Emax}$ 475 / 505 $\Phi_F$ n.a.

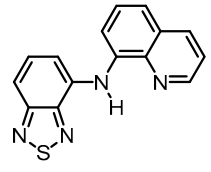

**BTD-QN**

Toluene / EtOH

$\lambda_{Amax}$ 440 / 450 $\varepsilon$ 7.8 / 6.2 × $10^3$

$\lambda_{Emax}$ 600 / 570 $\Phi_F$ 0.50 / 0.13

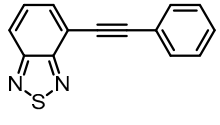

**BTD-CCPh**

Toluene / EtOH

$\lambda_{Amax}$ 367 / 366 $\varepsilon$ 14.1 / 15.1 × $10^3$

$\lambda_{Emax}$ 447 / 485 $\Phi_F$ 0.42 / 0.30

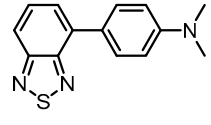

**LD-BTD1**

Toluene / MeOH

$\lambda_{Amax}$ 429 / 423 $\varepsilon$ 7.1 × $10^3$ (hexane)

$\lambda_{Emax}$ 578 / 709 $\Phi_F$ 0.71 / < 0.01

Figure 9. Examples of monosubstituted BTD derivatives used for LD-specific fluorescence imaging. Photophysical properties in toluene and alcohol solution (MeOH or EtOH) are indicated in grey.[60,121,125,126] n.a. = data not available; units: $\lambda_{Amax}$ and $\lambda_{Emax}$ in nm, $\varepsilon$ in $M^{-1}$ $cm^{-1}$.

The work described in the following Section 3.2 builds upon the reported compound **LD-BTD1** (Figure 9). A series of BTD derivatives with various 4-*N*-substituents (amines and amides) were synthesized and their photophysical properties were investigated. Direct attachment of the *N*-substituent on BTD was expected to increase the water solubility due to the absence of the lipophilic phenyl linker. The compounds were tested for their utility as fluorescence imaging agents in cancer cells, including to examine if LD-specific staining is maintained with the less lipophilic compounds (compared to **LD-BTD1**).

## 3.2 Results and discussion

### 3.2.1 Synthesis of 4-*N*-substituted benzothiadiazole derivatives

The commercially available 4-amino-BTD (**1**) served as substrate for methylation and acylation to give compounds **2**, **3** and **4**, **5**, respectively (Scheme 1). The low yields of the mono- and dimethylated derivatives **2** and **3** (~40%) can partially be explained by challenging purification along with volatile behavior of both compounds. Amide-substituted BTDs **4** and **5** were obtained via nucleophilic addition-elimination of **1** and the corresponding acyl chloride in 92% and 65% yield, respectively. Compound **1** itself was purified by sublimation prior to photophysical and cell imaging studies.

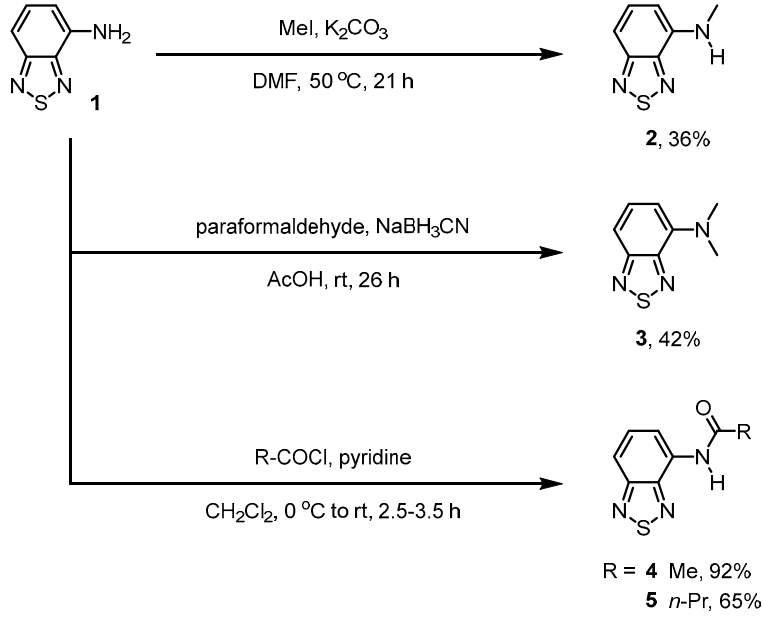


Scheme 1. Synthesis of 4-*N*-substituted BTD derivatives **2**–**5** starting from 4-amino-BTD (**1**). Me = methyl; DMF = *N*,*N*-dimethylformamide; AcOH = acetic acid; rt = room temperature; *n*-Pr = *normal*-propyl.

The remaining compounds in the series (**6–15**) were prepared from 4-bromo-BTD through cross-coupling reactions (Scheme 2). Palladium-catalyzed Buchwald-Hartwig aminations using PEPPSI-IPr and cyclic or primary amines afforded compounds **6–12** in moderate to high yields (54–85%). Using the same conditions for the synthesis of the diphenylamino derivative **13**, however, gave a very poor yield (6%). Alternatively, the $Pd_2(dba)_3$/RuPhos catalytic system was found to provide an improved yield of 35%. The amino acid derivatives **14** and **15** were synthesized via Ullmann-type coupling using copper(I) iodide in 26% and 36% yield, respectively.

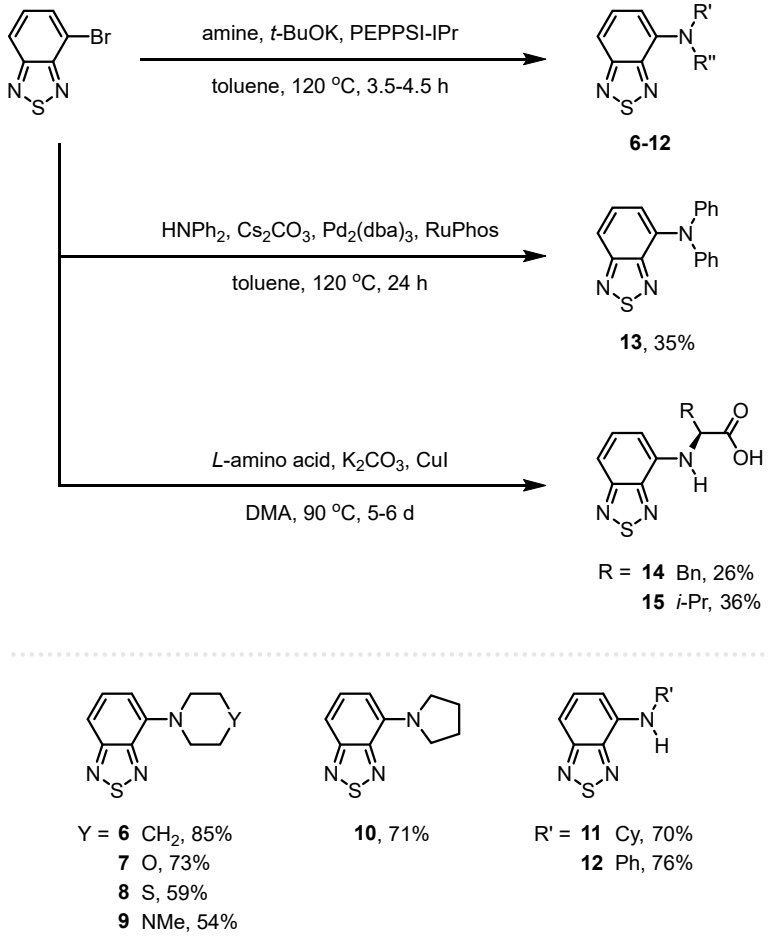


Scheme 2. Synthesis of 4-*N*-substituted BTD derivatives **6–15** via Buchwald-Hartwig aminations or Ullmann-type couplings starting from 4-bromo-BTD. *t*-BuOK = potassium *tert*-butoxide; DMA = *N*,*N*-dimethylacetamide; Bn = benzyl; *i*-Pr = *iso*-propyl; Cy = cyclohexyl; Ph = phenyl.

It should be noted that none of the reactions described above were optimized and there might be more efficient synthetic protocols. However, the main goal

was to obtain several milligrams of pure material for the photophysical characterization and cell studies.

### 3.2.2 Photophysical characterization

Before discussing the photophysical properties of the 4-*N*-substituted BTD derivatives (**1–15**), an honest mistake in the procedure of the fluorescence measurements needs to be disclosed. In Paper I, the appearance of dual emission in the spectra of the amides **4** and **5** in hexane is described, which was interpreted as fluorescence from the LE state and the ICT state. However, we recently discovered that this dual emission is not reproducible when the spectra are acquired using a different fluorometer (Figure 10A).

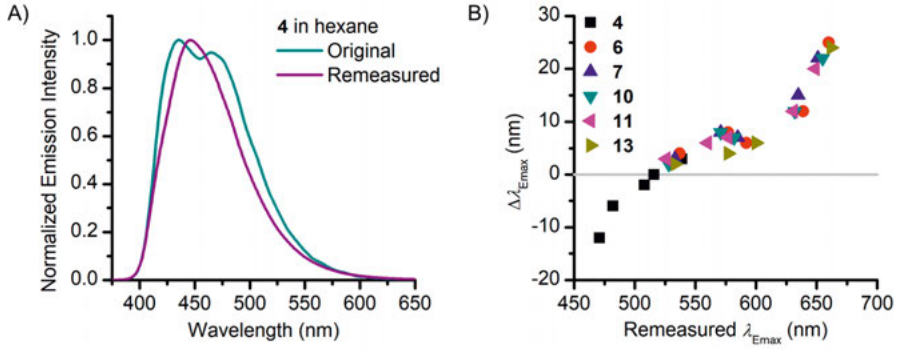


Figure 10. Comparison of original emission data in Paper I with remeasured data. A) Normalized emission spectra of the amido-BTD derivative **4** in hexane ($\lambda_{ex}$ = 360 nm); the original spectrum (in teal) shows two emission maxima in contrast to the remeasured spectrum (in purple). B) Absolute difference between remeasured and original $\lambda_{Emax}$ values ($\Delta\lambda_{Emax}$) of compounds **4**, **6**, **7**, **10**, **11**, and **13** in different solvents (hexane, toluene, THF, DMSO, and MeOH) plotted against the corresponding remeasured $\lambda_{Emax}$ values. The remeasured values below the grey line ($\lambda_{Emax}$ < 516 nm) are smaller than the original values, whereas the remeasured values above the grey line ($\lambda_{Emax}$ > 516 nm) are larger. The emission of compound **4** in hexane was not included in the plot due to the two maxima in the original data; instead, its emission in water (with 5% DMSO) was added.

The reason for the apparent dual emission in the original spectrum is presumably that the old instrument (that was used to record the fluorescence data in Paper I) had strong wavelength-dependent intensity variations in the fluorescence detection, which were not corrected appropriately in the acquired raw data. We suspect that a drop in the detected intensity close to the actual emission maximum of the amides (e.g., **4**, $\lambda_{Emax}$ = 447 nm in hexane) caused the apparent dual emission. Unfortunately, the old instrument is no longer accessible, so this hypothesis cannot be confirmed with absolute certainty. Nevertheless, this issue is currently being further investigated by remeasuring all compounds in Paper I on the new instrument, which automatically corrects

acquired raw data with correction factors provided by the manufacturer. An appropriate correction of Paper I will be submitted to the corresponding publisher in the near future.

The emission data for some of the 4-*N*-substituted BTD derivatives (**4**, **6**, **7**, **10**, **11**, and **13**) were remeasured in time to be included in this thesis (Table 1; remeasured emission spectra and further graphs are included in the Appendix). Figure 10B demonstrates the wavelength-dependent degree of deviation between the remeasured and the original $\lambda_{Emax}$. The more the emission maximum diverges from 516 nm, the larger the difference between the original and remeasured data. Remeasured values with $\lambda_{Emax} < 516$ nm are smaller than the original values, whereas remeasured values with $\lambda_{Emax} > 516$ nm are larger. Accordingly, compounds **6** and **13**, which have the most red-shifted emission maxima in the series ($\lambda_{Emax} = 660$ and 662 nm, respectively), showed the largest deviation ($\Delta\lambda_{Emax} = 25$ and 24 nm, respectively). Moreover, the remeasured fluorescence quantum yields showed varying deviations from the original data (e.g., **7**, $\Phi_{F,remeasured} = 0.49$ and 0.40 vs $\Phi_{F,original} = 0.50$ and 0.32 in toluene and THF, respectively). Importantly, the general photophysical trends, observed for the original data, are the same as in the remeasured data. Emission-related values of compounds (i.e., $\lambda_{Emax}$, $\Phi_F$, and Stokes shift) that are stated in the following discussion refer to remeasured data.

The photophysical properties of compounds **1–15** were investigated by UV-vis absorption and fluorescence spectroscopy in a variety of solvents of different polarity: hexane, toluene, tetrahydrofuran (THF), dimethyl sulfoxide (DMSO), methanol (MeOH), and water. The amino-BTD derivatives (**1–3** and **6–15**) feature more red-shifted emission in all studied solvents than the amides (**4** and **5**), in accordance with their stronger electron-donating nature. The $\lambda_{Emax}$ and the generally large Stokes shifts of all compounds increase with solvent polarity (e.g., Stokes shift = 75–187 nm / 4510–9856 $cm^{-1}$ for **4** and 130–249 nm / 6052–9515 $cm^{-1}$ for **7**). The solvatochromic emission spectra of compounds **4** and **7** are depicted in Figure 11.

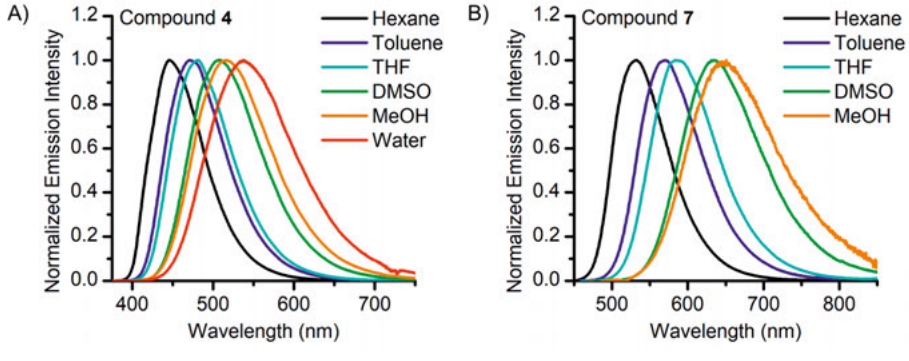


Figure 11. Normalized emission spectra of the amido-BTD derivative **4** (A) and the amino-BTD derivative **7** (B) in various solvents (remeasured data), showing positive solvatochromism. The spectrum of **7** in water is missing due to quenched emission.

Table 1. Photophysical data of compounds **4**, **6**, **7**, **10**, **11**, and **13**, remeasured using a Shimadzu RF-6000 fluorometer. Acquired raw data was automatically corrected for wavelength-dependent intensity variations (correction factors provided by the manufacturer).

| Compd. | Solvent | $\lambda_{Emax}$ (nm) | Stokes shift (nm / $cm^{-1}$) | $\Phi_F$[a] |
|---|---|---|---|---|
| **4** | Hexane | 447 | 75 / 4510 | 0.46 |
| | Toluene | 471 | 97 / 5507 | 0.64 |
| | THF | 482 | 108 / 5991 | 0.64 |
| | DMSO | 508 | 135 / 7125 | 0.58 |
| | MeOH | 516 | 154 / 8244 | 0.14 |
| | $H_2O$[b] | 539 | 187 / 9856 | 0.02 |
| **6** | Hexane | 537 | 124 / 5591 | 0.52 |
| | Toluene | 577 | 157 / 6479 | 0.46 |
| | THF | 592 | 172 / 6918 | 0.35 |
| | DMSO | 639 | 216 / 7991 | 0.13 |
| | MeOH | 660 | 247 / 9062 | <0.01 |
| **7** | Hexane | 533 | 130 / 6052 | 0.61 |
| | Toluene | 571 | 162 / 6937 | 0.49 |
| | THF | 585 | 177 / 7416 | 0.40 |
| | DMSO | 635 | 223 / 8524 | 0.15 |
| | MeOH | 651 | 249 / 9515 | <0.01 |
| **10** | Hexane | 528 | 82 / 3482 | 0.44 |
| | Toluene | 571 | 113 / 4321 | 0.42 |
| | THF | 582 | 125 / 4700 | 0.35 |
| | DMSO | 632 | 168 / 5729 | 0.12 |
| | MeOH | 655 | 196 / 6519 | <0.01 |
| **11** | Hexane | 526 | 95 / 4190 | 0.51 |
| | Toluene | 560 | 122 / 4974 | 0.33 |
| | THF | 577 | 135 / 5293 | 0.29 |
| | DMSO | 631 | 180 / 6325 | 0.05 |
| | MeOH | 649 | 206 / 7165 | <0.01 |
| **13** | Hexane | 533 | 85 / 3560 | 0.42 |
| | Toluene | 577 | 124 / 4744 | 0.27 |
| | THF | 600 | 149 / 5506 | 0.17 |
| | DMSO | 662 | 211 / 7067 | 0.02 |
| | MeOH | n.e. | n.e. | n.e. |

[a] $\Phi_F$ of **4** was determined relative to quinine sulfate in 0.05 M aq. $H_2SO_4$ ($\Phi_F$ = 0.55)[14], $\lambda_{ex}$ = 360 nm; $\Phi_F$ of **6**, **7**, **10**, **11**, and **13** was determined relative to fluorescein in 0.1 M aq. NaOH ($\Phi_F$ = 0.93)[14], $\lambda_{ex}$ = 450 nm (**6**, **7**, **10**, **11**) or 460 nm (**13**). [b] With 5% DMSO. n.e. = no emission detected.

Lippert-Mataga plots[9,10] represent the correlation between Stokes shifts and the solvent orientation polarizability parameter. The Lippert-Mataga plots of all studied compounds show large positive gradients, which is true for both the original and remeasured data. This indicates a significant increase in dipole moment upon excitation, which is expected for emission from fluorophores that undergo ICT in the excited state. In general, a better linearity was observed for correlations between Stokes shifts and Reichardt's $E_T(30)$ solvent polarity parameter[127] as opposed to the orientation polarizability parameter[9,10] (the new graphs are included in the Appendix).

The fluorescence quantum yields of BTD derivatives with an amine substituent (**1–3** and **6–15**) decrease with increasing solvent polarity (e.g., **6**, $\Phi_F = 0.52$ in hexane and $\Phi_F = 0.13$ in DMSO). A linear correlation was found between $\Phi_F$ values and the $E_T(30)$ solvent polarity parameter[127] in aprotic solvents. In MeOH, the compounds are barely emissive ($\Phi_F \leq 0.01$). The derivatives with a weaker electron-donating amide substituent (**4** and **5**) retain a high quantum yield in DMSO ($\Phi_F = 0.58$ for **4**) but also decrease in protic solvents. The fluorescence decrease, however, is less pronounced compared to the amines, with **4** retaining fluorescence in MeOH and even in aq. solution ($\Phi_F = 0.14$ and 0.02, respectively). Fluorescence quenching in protic solvents is a common phenomenon that affects many fluorophores. Different possible explanations have been discussed in literature, including hydrogen bonding effects and through space energy transfer from the excited fluorophore to solvent vibrational stretching modes ($\lambda > 600$ nm).[128]

Comparison of dimethylamino-BTD **3** (original data) with **LD-BTD1** (data taken from the literature)[126] reveals that the phenyl linker has significant influence on the photophysical properties. Similar $\lambda_{Amax}$ were observed for both compounds, whereas the emission maxima of **3** were more blue-shifted. The molar extinction coefficient of **LD-BTD1** ($\varepsilon = 7100\ M^{-1}\ cm^{-1}$)[126] was nearly twice as high as for **3** ($\varepsilon = 3600\ M^{-1}\ cm^{-1}$) in hexane, which could be expected due to the extended conjugated system. The fluorescence quantum yield in apolar solvents was also significantly larger for **LD-BTD1**, while a comparable quenching behavior in polar solvents was observed.

In analogy to the emission maxima, the $\lambda_{Amax}$ of the studied amino-BTD derivatives (**1–3** and **6–15**) were generally more red-shifted than the absorption of the amides (**4** and **5**), ranging between 380–464 nm and 352–375 nm, respectively. The amino-BTD derivatives showed small bathochromic shifts of $\lambda_{Amax}$ with increasing solvent polarity in aprotic solvents (for example **7**, $\lambda_{Amax}$ = 403 and 412 nm in hexane and DMSO, respectively). Stronger hypsochromic shifts were observed in polar protic solvents for tertiary amines **3** and **6–9** (for example **7**, $\lambda_{Amax}$ = 402 and 380 nm in MeOH and water, respectively). This phenomenon often occurs with aromatic amines and is commonly ascribed to hydrogen bonding effects between the nitrogen lone pair and the solvent.[129,130] The ability of primary and secondary amines to act as hydrogen bond donors typically mitigates this

effect. The absorption maximum of the diphenylamino derivative **13**, in which the nitrogen lone pair is delocalized over three aromatic rings, remained nearly constant in all solvents. Another exception was the pyrrolidine derivative **10**, which exhibited a red-shifted absorption maximum in water ($\lambda_{Amax}$ = 460 nm) compared to hexane ($\lambda_{Amax}$ = 446 nm). In general, the red-shifted $\lambda_{Amax}$ of **10** in all solvents compared to the other compounds stood out (for example **10**, $\lambda_{Amax}$ = 446 nm and **6**, $\lambda_{Amax}$ = 413 nm in hexane). Density functional theory (DFT) calculations indicated a flattened geometry around the nitrogen atom and relative to BTD, as compared to the piperidine derivative **6** (Figure 2 in Paper I). This might allow better conjugation of the nitrogen lone pair of **10** with the BTD π-system, which is also reflected in its higher molar extinction coefficient (for example **10**, $\varepsilon$ = 5000 $M^{-1}$ $cm^{-1}$ and **6**, $\varepsilon$ = 3000 $M^{-1}$ $cm^{-1}$ in toluene). Compounds containing an aromatic ring as substituent on the amine, in addition to BTD (i.e., **12** and **13**), featured higher $\varepsilon$ than compounds with aliphatic substituents (e.g., **12**, $\varepsilon$ = 6300 $M^{-1}$ $cm^{-1}$ and **11**, $\varepsilon$ = 3500 $M^{-1}$ $cm^{-1}$ in hexane). Comparing the aniline derivative **12** with **LD-BTD1**[126] shows that the molar extinction coefficient is marginally increased when the phenyl ring is placed as a linker between the acceptor and the donor (7100 $M^{-1}$ $cm^{-1}$ for **LD-BTD1** in hexane[126]).

The compounds that proved useful for cell imaging, **11–13** (see below, Section 3.2.3), were further investigated. Their photostability was examined in toluene. Compound **13** showed excellent photostability while the emission intensity of **11** and **12** decreased by about 15% after 30 min of irradiation in the fluorometer with maximum excitation slit width (i.e., 20 nm bandwidth). Furthermore, compounds **11–13** were examined for their aggregation behavior in DMSO/water mixtures with increasing fractions of water. The emission intensity of compounds **11** and **12** quickly decreased with increasing water fractions, which is in line with the generally observed fluorescence quenching in protic solvents (discussed above). Compound **13** initially showed a similar behavior, however, the emission was significantly increased with 90% and 95% water content. The sudden emission increase in mixtures with high water content is most likely due to aggregation induced emission, which is a common behavior of lipophilic BTD derivatives.[125,131-134]

### 3.2.3 Fluorescence imaging of cancer cells

The BTD derivatives **1–15** were examined as potential probes for fluorescence cell microscopy. The compounds were tested in melanoma (SK-MEL-28) and breast cancer (MDA-MB-231) cells. After an initial screening of all compounds, the cell imaging studies were focused on compounds **11–13**, which showed a bright and clear punctuate fluorescence pattern in the cells (**12** shown in Figure 12A). Immunofluorescence colocalization of **11–13** with an antibody for the LD-associated adipose differentiation-related protein (ADFP) confirmed LD-specific staining in both cell lines (Figure 3 in Paper I). In addition, fluorophores **11–13** could visualize increased accumulation and growth of LDs in cancer cells after oleic acid supplementation (Figure 12), which is a known method to stimulate LD formation.[135-137]

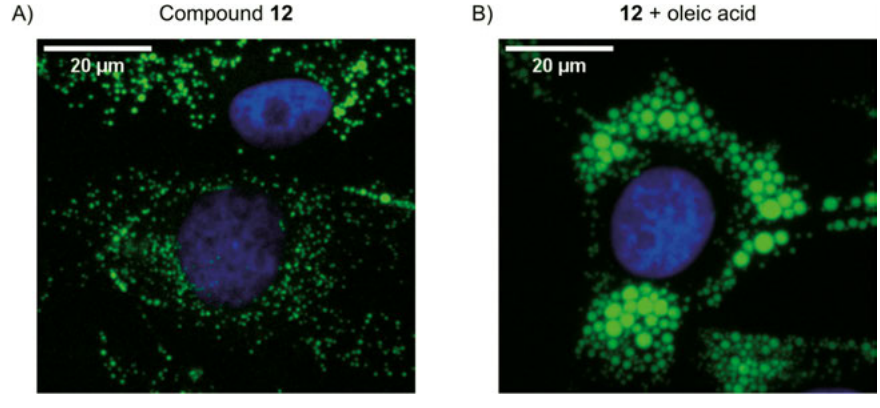


Figure 12. Fluorescence microscopy images of SK-MEL-28 cells stained with **12** (seen in green; $\lambda_{ex}$ = 460–500 nm, $\lambda_{em}$ = 512–542 nm). Staining was performed on fixed cells (10 µM, 1 h incubation). Cell nuclei are stained with **DAPI** (4',6-diamidino-2-phenylindole; seen in blue; $\lambda_{ex}$ = 325–375 nm, $\lambda_{em}$ = 435–485 nm). A) Cells without lipid supplementation. B) Cells treated with oleic acid (100 µM, 24 h incubation) before fixation.

The cell viability of SK-MEL-28 and MDA-MB-231 cells was examined using the Resazurin assay.[138] Treatment of the cells with **11** or **12** (10 µM, 24 h incubation) resulted in no significant cytotoxicity. However, treatment with compound **13**, using the same conditions, showed strong variations in the cell viability results when comparing multiple repetitions of the experiment. These unclear results can presumably be ascribed to a sensitive aggregation behavior of **13** (as seen in the photophysical experiments). As cytotoxicity could not be ruled out, the probe is consequently recommended for use on fixed cells only.

### 3.2.4 Lipophilicity

The lipophilicity of a compound can be defined by the logP, which is the logarithmic octanol/water partition coefficient. The logP value can either be negative or positive, indicating preferred partitioning in the aq. phase or the organic phase, respectively. For example, the calculated logP[139] for the acetate anion is −1.6 and for dodecyl acetate 5.9. The logP values of nine compounds (**1–5**, **7**, **9**, **14**, **15**) were experimentally determined and compared to calculated data based on the structures.[139] The calculated values were considered a good approximation since they only deviated from the experimental data by $\Delta\log P \leq 0.6$. As the experimental logP determination of very lipophilic compounds is challenging, only calculated logP values were acquired for the more lipophilic compounds. The three compounds **11–13** that showed LD-specific staining had calculated logP values of 4.4, 4.0 and 5.5, respectively, representing the most lipophilic compounds of the studied BTD derivatives. All other compounds (**1–10**, **14**, and **15**) had calculated $\log P \leq 3.0$. In Table 2, the logP values are presented in comparison with other published LD-specific fluorophores that are mentioned in this thesis.

Table 2. Calculated logP values of fluorophores with LD-specific staining. Left column: compounds in this work (**11–13**); middle column: other BTD-based fluorophores (from Section 3.1.2); right column: fluorophores not based on BTD (from Section 1.4.2 and including compound **17** from Paper III).

| Compd. | Calcd. logP[a] | Compd. | Calcd. logP[a] | Compd. | Calcd. logP[a] |
|---|---|---|---|---|---|
| **11** | 4.4 | **LD-BTD1**[126] | 3.9 | **Nile Red** | 4.6 |
| **12** | 4.0 | **BTD-AO**[60] | 8.8 | **Oil Red O** | 8.6 |
| **13** | 5.5 | **BTD-QN**[121] | 3.9 | **17** (Paper III) | 4.0 |
| | | **BTD-CCPh**[125] | 3.4 | | |

[a] Calculated logP values obtained using the Molinspiration Cheminformatics web service.[139]

This overview indicates that LD-specific fluorescent probes typically have a logP of 4 or higher. It was previously reported that $\log P > 5$ is usually required for reasonably good LD staining and many fluorescent probes for LDs even reach far beyond that value.[140,141] However, apart from lipophilicity, the photophysical properties are also relevant to consider for successful use in fluorescence microscopy. Sufficient brightness in a lipophilic environment is by all means required and strong fluorescence quenching in an aq. environment is certainly beneficial if the probe is not very lipophilic and does not tend to solely accumulate in LDs.

One interesting example, that does not follow the lipophilic trend, is the small disubstituted BTD derivative **CBD-Fluor** (Figure 13).[99,142] The compound **CBD-Fluor** can successfully be applied for LD imaging despite a low calculated logP of 1.6.[142] The authors did not elaborate on this in the

publication. The fluorescence quenching in water may contribute to its LD imaging. However, methylamino-BTD **2** and many of the other 4-*N*-substituted derivatives in Paper I also exhibit this beneficial photophysical property in combination with low logP values. Nevertheless, they showed weak and rather unspecific staining in cells instead of clear and bright LD-specific staining as reported for **CBD-Fluor**.

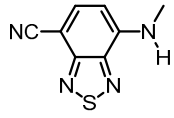

Toluene / water

$\lambda_{Amax}$ 435 / 441 $\varepsilon$ 4.4 / 3.0 × $10^3$

$\lambda_{Emax}$ 532 / 612 $\Phi_F$ 0.30 / 0.005

**CBD-Fluor** Calculated logP = 1.6

Figure 13. Structure and photophysical properties of **CBD-Fluor**, an LD-specific BTD derivative reported by Lukesh III and co-workers.[142] Photophysical data (indicated in grey) taken from the literature.[142] LogP value obtained using the Molinspiration Cheminformatics web service.[139]

## 3.3 Summary

The work discussed in this Chapter contributed to a better understanding of the structure-photophysical property and structure-LD-specificity relationships of fluorescent 4-*N*-substituted BTD derivatives. Three compounds, **11**–**13**, were identified as LD-specific fluorescent probes applicable for cell imaging (Figure 14). Compound **13** was recommended for staining fixed cells only due to possible cytotoxicity.

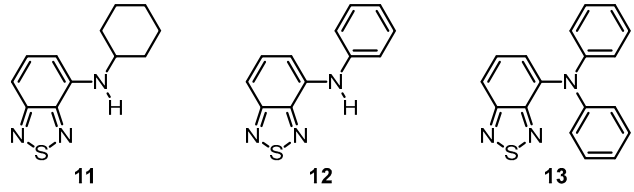

**11** **12** **13**

$\lambda_{Amax}$ 438 nm $\lambda_{Amax}$ 439 nm $\lambda_{Amax}$ 453 nm

$\lambda_{Emax}$ 560 nm $\lambda_{Emax}$ 547 nm $\lambda_{Emax}$ 577 nm

Figure 14. New BTD-based fluorescent probes specific for LDs presented in this work (Paper I). Maximum absorption and emission wavelengths ($\lambda_{Amax}$ and remeasured $\lambda_{Emax}$) in toluene are shown.

Strongly electron-donating amine substituents (as in **1**–**3** and **6**–**15**) caused red-shifted absorption and emission compared to amide substituted BTD derivatives (**4** and **5**). All studied compounds showed fluorescence quenching in aq. environment and very large solvent-dependent Stokes shifts, the latter being a favorable property for fluorescence imaging applications as it

contributes to background reduction. The majority of the compounds with amino moieties directly attached to BTD showed reduced lipophilicity and thus improved water solubility, compared to **LD-BTD1**[126]. However, bright LD-specific staining was only achieved with compounds **11–13**, which are equally or more lipophilic (logP ≥ 4) than **LD-BTD1**, indicating a general predictive value of lipophilicity towards accumulation of BTD-based fluorophores in LDs.

This work revealed three new BTD-based fluorescent probes for imaging LDs in cancer cells. As LDs play a crucial role in the energy metabolism, these fluorophores are important tools in the field of cancer cell biology.

# 4 Fluorescent indoline derivatives: A small structural difference with great impact on photophysical and cell imaging properties (Papers II and III)

## 4.1 Background

In contrast to the electron-deficient nature of BTD, the indoline structure (Figure 15), which comprises a cyclic amine, can be employed as an electron-donating unit in D-A fluorophores.[143,144] The smallest possible indoline-based D-A systems incorporate an EWG, such as a ketone, at the C3 carbon. The natural product and popular **Indigo dye** is one example of such an indolin-3-one derivative (Figure 15).[145,146] 2,2-Disubstituted indolin-3-ones are often referred to as pseudoindoxyls. A few *N*-substituted pseudoindoxyls have been applied as fluorescent probes, such as **LipidGreen** and **LipidGreen2** (Figure 15) that can be used for imaging intracellular lipids.[147-152]

Instead of a ketone, an imine moiety can also be integrated into indolines as an EWG. The indolin-3-imine scaffold can be found in natural products and 2,2-disubstituted derivatives are also synthetically accessible.[153-159] However, as opposed to indolin-3-ones, the fluorescent properties of the imine derivatives and associated potential applications have not been further investigated in literature.

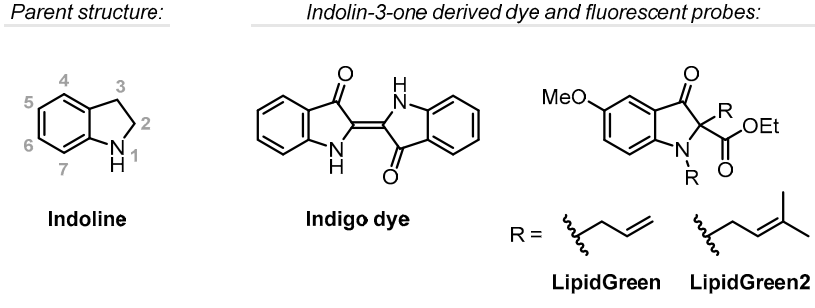


Figure 15. Structures of indoline (atom numbers indicated in grey), **Indigo dye**, and **LipidGreen** fluorophores.

The indolin-3-imine derivative **16** (Figure 16) was the compound of choice for the photophysical and cell imaging study in Paper II. Its synthesis has recently been reported by Streuff and co-workers.[156] Considering the possibility that imines can be hydrolyzed in a cellular environment, the novel ketone analogue **17** (Figure 16) was initially synthesized as a hydrolysis control for the cell imaging experiments. However, the compounds indeed behaved differently and, on top of that, indolin-3-one **17** featured interesting characteristics, which were further investigated in Paper III. The following Sections in this Chapter compose a joint summary, comparing the photophysical, (photo)chemical and cell imaging behavior of these two structural analogues.

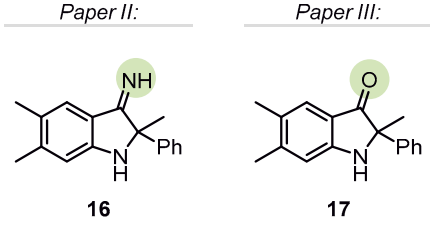


Figure 16. Structures of the indoline derivatives (**16** and **17**) studied in Papers II and III.

## 4.2 Results and discussion

### 4.2.1 Photophysical characterization

The photophysical properties of indolin-3-imine **16** and indolin-3-one **17** (Figure 16) were initially investigated in toluene, DMSO, and MeOH. The results are summarized in Table 3.

Table 3. Photophysical characterization data of **16** and **17** in different solvents.

| Compd. | Solvent | Band | $\lambda_{Amax}$ (nm) | $\lambda_{Emax}$ (nm) | Stokes shift (nm/$10^3$ $cm^{-1}$) | $\varepsilon$ ($M^{-1}$ $cm^{-1}$) | $\Phi_F$[a] |
|---|---|---|---|---|---|---|---|
| **16** | Toluene | | 365 | 417 | 52 / 3.4 | 4500 | 0.03 |
| | DMSO | | 379 | 441 | 62 / 3.7 | 4000 | 0.15 |
| | MeOH | A | 400[b] | 533[c] | 133 / 6.2[b] | - | 0.10 |
| | | B | 443[b] | 533[d] | 90 / 3.8[b] | - | 0.21[d] |
| **17** | Toluene | | 383 | 434 | 51 / 3.1 | 3800 | 0.16 |
| | DMSO | | 401 | 463 | 62 / 3.3 | 4300 | 0.41 |
| | MeOH | | 402 | 487 | 85 / 4.3 | 3900 | 0.30 |

[a] $\lambda_{ex}$ = 360 nm unless indicated otherwise. [b] Two absorption bands with concentration-dependent intensity ratio were observed. Data given here is derived from a 25 µM sample solution. [c] $\lambda_{ex}$ = 360 nm; a weak shoulder was observed at ~450 nm. [d] $\lambda_{ex}$ = 450 nm.

Both compounds showed positive solvatochromic absorption and emission maxima as well as Stokes shifts that increased with solvent polarity. The $\lambda_{Amax}$ and $\lambda_{Emax}$ of **17** in the aprotic solvents were bathochromically shifted by around 20 nm compared to **16**, likely due to the stronger electron-withdrawing nature of the carbonyl group. In MeOH, on the other hand, the emission of **16** was exceptionally red-shifted ($\lambda_{Emax}$ = 533 nm) and the absorption featured two bands ($\lambda_{Amax}$ = 400 and 443 nm at 25 µM concentration) in the visible spectrum (Figure 17).

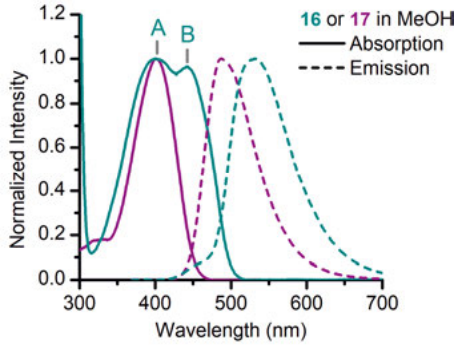


Figure 17. Normalized absorption (solid lines) and emission (dashed lines) spectra of **16** (teal) and **17** (purple) in MeOH (25 µM). The A-band and B-band are indicated.

The effect of additives and different protic solvents on the absorption spectrum of **16** are discussed in the following Section (4.2.2), in which the two bands are referred to as the A-band and the B-band (as indicated in Figure 17). The molar extinction coefficients of **16** and **17** were similar, ranging from 3800–4500 $M^{-1}$ $cm^{-1}$. On the contrary, the fluorescence quantum yield was significantly increased in the polar solvents as compared to toluene (e.g., **17**, $\Phi_F$ = 0.16 in toluene and 0.41 in DMSO), with both compounds following a similar trend. Interestingly, **17** was generally more emissive than **16** (~3–5 times higher $\Phi_F$), indicating less efficient non-radiative relaxation of its excited states.

### 4.2.2 pH Sensitivity studies of indolin-3-imine **16**

The intensity ratio between the two absorption bands of **16** in MeOH (Figure 17) could be influenced in several ways. The A-band ($\lambda_{Amax} \leq 400$ nm) gained dominance at concentrations above 25 µM (Figure 18A), whereas the B-band increased upon addition of water to the solution (Figure 1E in Paper II). Interestingly, when water was added to a solution of **16** in DMSO, a second, red-shifted absorption band appeared, comparable to the B-band of the compound in MeOH (Figure 18B).

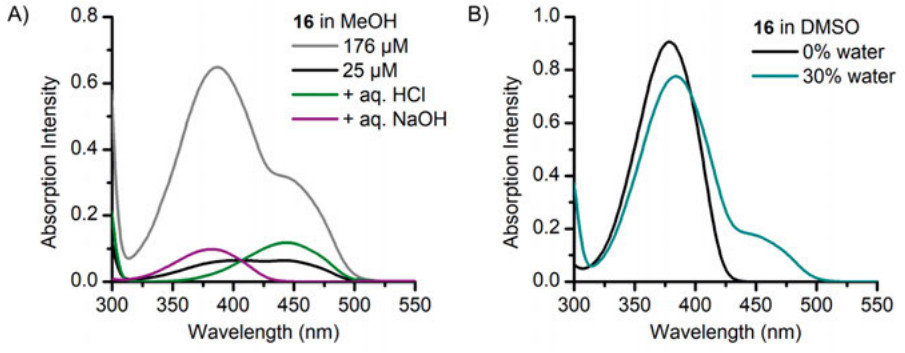


Figure 18. A) Concentration-dependent absorption spectra of **16** in MeOH (grey and black lines) and influence of excess acid (green line) or base (purple line) on the spectra (25 µM **16**, 0.2 mM aq. HCl or NaOH). B) Influence of water fraction (30%) on the absorption spectra of **16** (0.2 mM) in DMSO.

To confirm that the protic nature of water was responsible for these effects, MeOH fractions were added to a solution of **16** in DMSO, which also caused the appearance and increase of the B-band (not shown). However, higher MeOH fractions were needed to obtain similar A-band/B-band absorbance ratios as compared to water. These results were indicative of a ground state equilibrium of **16** in polar protic solvents or solvent mixtures, involving a proton transfer.

Further experiments in MeOH and DMSO using acid or base additives (aq. HCl or aq. NaOH), revealed that acid shifted the ground state equilibrium entirely to the B-band species while base shifted the equilibrium entirely to the A-band species (Figure 18A). The gap between the two absorption maxima was $\Delta\lambda_{Amax}$ = 62 nm (0.46 eV), which was close to the results of time-dependent DFT calculations of **16** and its protonated form (**16H**$^+$) in MeOH (using the polarizable continuum model for solvation), which gave $\Delta\lambda_{Amax}$ = 40 nm (0.35 eV).

Nuclear magnetic resonance (NMR) spectroscopy (one- and two-dimensional) confirmed protonation of the imine when aq. HCl was added to the NMR sample of **16** in DMSO-$d_6$. The stacked $^1$H NMR spectra in Figure 19 show a general downfield shift of the resonance signals upon acid addition and conversion of the broad imine NH peak into two much sharper peaks.

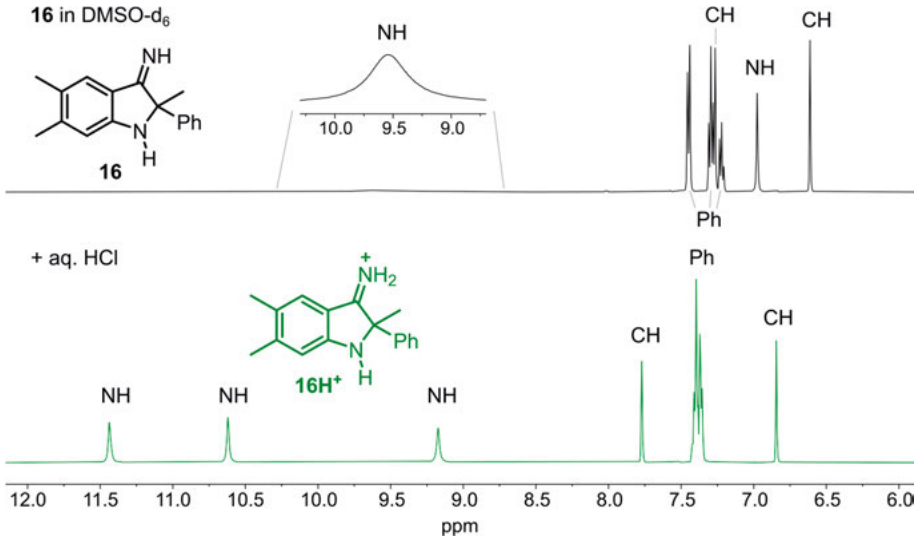


Figure 19. Aromatic region of the $^{1}$H NMR spectrum (500 MHz) of **16** (0.03 M) in DMSO-$d_6$ (top) and after addition of aq. HCl (bottom; ~1.5 equivalents, final water content: 1%).

The p$K_a$ of protonated **16** (**16H**$^+$) in the ground state was determined based on changes in the absorption spectra at different pH (2–12) in aq. buffer solution (Figure 20). The resulting pH curve gave a p$K_a$ of 8.3±0.1. This value indicates weak basicity of the imine, which is very similar to the reported p$K_a$ of protonated 2,4-dimethoxy-benzophenone imine (p$K_a$ = 8.3[160]) and only one unit lower than the p$K_a$ of 4-aminopyridinium (p$K_a$ = 9.2[161]).

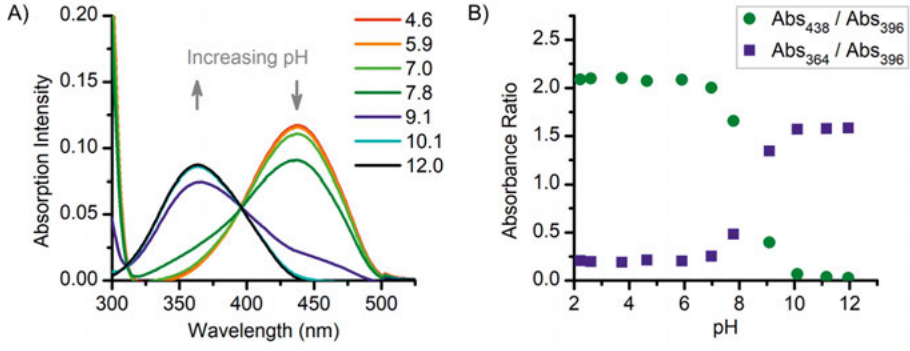


Figure 20. A) pH-Dependent absorption spectra of **16** (25 µM) in Britton-Robinson buffer (with 1% DMSO). B) pH Curves based on the absorbance ratio of **16** (blue, $\lambda_{Amax}$ = 364 nm) or **16H**$^+$ (green, $\lambda_{Amax}$ = 438 nm) and the isosbestic point ($\lambda$ = 396 nm).

The emission spectrum of **16** in MeOH showed excitation wavelength-dependent variations. Excitation within the B-band ($\lambda_{ex}$ = 450 nm) resulted in a single emission band ($\lambda_{Emax}$ = 533 nm), whereas excitation within the A-band

($\lambda_{ex}$ = 360 nm) revealed a weak, blue-shifted shoulder in the emission spectrum (see Figure 17 on page 40). Examination of the corresponding excitation spectra confirmed that both ground state species (**16** and **16H**$^+$) contribute to the major emission band, while the weak shoulder arises exclusively from the A-band species **16** (Figure S4 in Paper II Supporting Information). These results indicate that, in addition to the ground state equilibrium, **16** is involved in an excited state proton transfer (ESPT) in MeOH, which presumably proceeds faster than the fluorescence from the excited state **16**$^*$.

In analogy to the p$K_a$ of a compound in the ground state, the rate of proton transfer in the excited state is affected by its excited state acidity (p$K_a^*$). Molecules that are more acidic in the excited state (p$K_a^*$ < p$K_a$) are called photoacids, while an enhanced basicity (p$K_a^*$ > p$K_a$ of the conjugate acid) is characteristic for photobases. Photoacids have been studied for nearly a century.[12,162-165] Photobases, however, have received remarkably less attention.[166] An approximate value of the p$K_a^*$ of a compound can be obtained according to the thermodynamic Förster cycle, when the p$K_a$ and the 0-0 transition energies of the acid and its conjugate base are known.[12,167,168] The latter refers to the energy difference between the vibrational ground states (v = 0) of $S_0$ and $S_1$, which can be estimated from the intersection of the normalized absorption and emission spectrum of the corresponding compound. It should be noted that in the following discussion about photobases (including Figure 21), the p$K_a$ and p$K_a^*$ refer to their conjugate acids. The Förster cycle of a general photobase and the derived equation to calculate p$K_a^*$ are shown in Figure 21.[12,166,167]

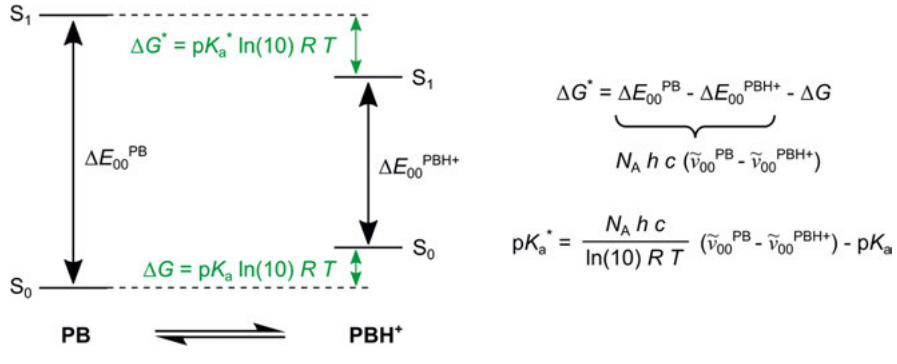


Figure 21. Schematic Förster cycle of a photobase (**PB**) and its conjugate acid (**PBH**$^+$) and derived equation for p$K_a^*$ approximation. $^*$ indicates excited state; $^{PB}$ and $^{PBH+}$ indicate base and conjugate acid, respectively; $\Delta G$ = Gibbs free energy change; $\Delta E_{00}$ = 0-0 transition energy; $\tilde{\nu}_{00}$ = wavenumber of 0-0 transition; $N_A$ = Avogadro constant; $h$ = Planck constant; $c$ = speed of light; $R$ = universal gas constant; $T$ = temperature.

The wavenumbers of the 0-0 transitions of **16** and **16H**$^+$ were obtained from sample solutions in 1 M aq. NaOH and 1 M aq. HCl, respectively. According

to the equation shown in Figure 21, an excited state acidity p$K_a^*$ of approximately 14 was calculated for the protonated imine **16H**$^+$. Hence, the basicity of **16** increases by around six orders of magnitude ($\Delta pK_a = 6$) upon photoexcitation. Among photobases studied in literature to date, $\Delta pK_a$ as low as 1[169] and as high as 14[168] have been reported. Some of the most studied photobases are 5-substituted quinolines, for which the $\Delta pK_a$ can be tuned from 2.2 through 5.9 to 10.6 when changing from an electron-withdrawing cyano group through a chloride to a donating amino group.[170]

The effects of the photobasicity of **16** on its emission spectra can be visualized in alcoholic solvents with different acidity (Figure 22). As described above, the emission spectrum recorded in MeOH almost exclusively shows the band ascribed to **16H**$^+$. In ethanol (EtOH), major emission from the band ascribed to **16** prevails and the A-band dominates in the absorption spectrum. In *iso*-propanol (*i*-PrOH), both spectra (absorption and emission) only show the band ascribed to **16**. Hereby, *i*-PrOH is representative for longer chain alcohols, as *n*-butanol and *n*-octanol showed very similar behavior, indicating that none of these alcohols is acidic enough to be deprotonated by **16** or **16**$^*$ to an observable extent.

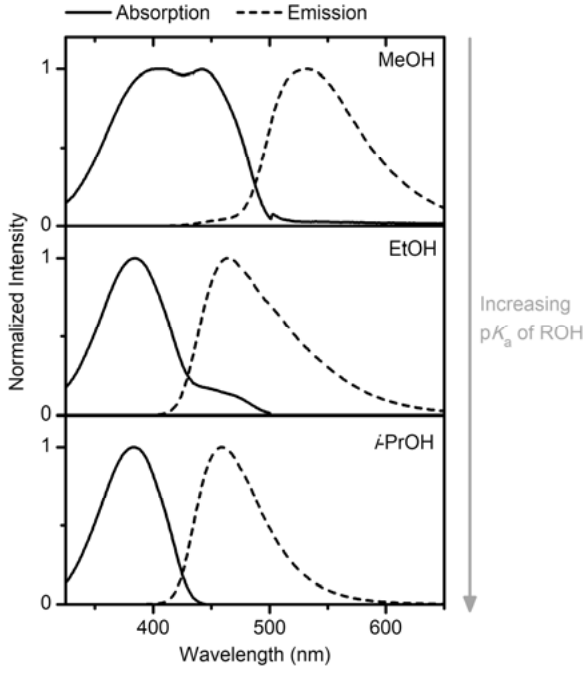


Figure 22. Normalized absorption (solid line) and emission (dashed line) spectra of **16** (25 µM) in different alcohols (ROH). The spectra are arranged with increasing alcohol p$K_a$ from top to bottom; p$K_a$ (in water) = 15.5 (MeOH), 15.9 (EtOH), 16.5 (*i*-PrOH).[171,172] $\lambda_{ex}$ = 404 nm (MeOH) or 384 nm (EtOH and *i*-PrOH).

The proposed ground and excited state processes of **16** are depicted in Scheme 3. In aprotic solvents (such as toluene or DMSO), only the neutral species are present (**16** and, after photoexcitation, **16**$^{*}$). Its solvatochromic emission is indicative of an ICT in the excited state before fluorescence occurs. Excited states with pronounced charge transfer character are typical for strong photoacids and -bases.[12] In sufficiently acidic protic solvents (such as MeOH or EtOH), the neutral imine is in equilibrium with its protonated form **16H**$^{+}$. When **16H**$^{+}$ is excited selectively, emission from its LE state is observed ($\lambda_{Emax}$ is independent of solvent polarity). On the other hand, when the neutral species **16** is excited selectively, the fluorescence is faced with a competing process, namely ESPT, resulting in **16H**$^{+*}$ from which bathochromic fluorescence occurs. As qualitatively indicated in Figure 22, the ESPT rate can be influenced by solvent acidity. This result is in line with Hunt and Dawlaty's studies of the photobase 5-methoxyquinoline, which also showed sensitive behavior towards various alcohols with an ESPT rate increase in more acidic alcohols.[172]

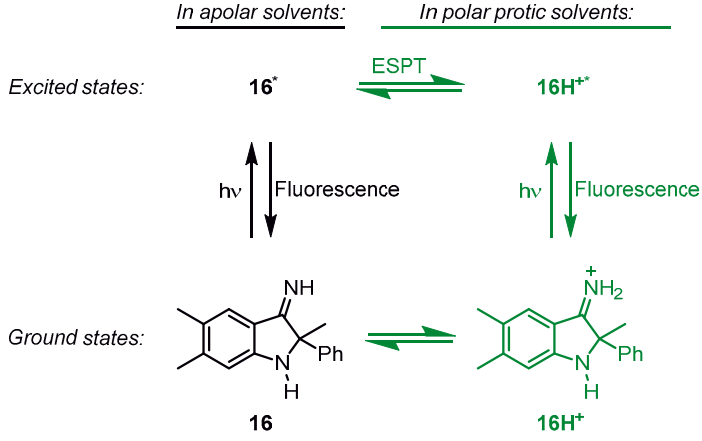


Scheme 3. Proposed ground and excited state processes of **16**. The left part of the scheme (in black) shows the photophysical processes in apolar solvents. Polar protic solvents enable proton transfer, resulting in a new emissive species (illustrated in green). ESPT = excited state proton transfer.

Furthermore, the equilibrium between **16** and **16H**$^{+}$ in deuterated methanol ($CD_3OD$) was shifted towards the neutral species, which can likely be explained with the slightly higher p$K_a$ of deuterated solvents compared to non-deuterated solvents.[173,174] More importantly, when the neutral species was excited in $CD_3OD$, the intensity ratio between the shoulder and the major emission band was increased (~1.7-fold) as compared to MeOH (Figure S5 in Paper II Supporting Information). This result agrees with the proposed ESPT as the kinetic isotope effect slows down the proton transfer.

As opposed to **16**, the initial photophysical characterization of indolin-3-one **17** (as described in Section 4.2.1) did not indicate an exceptional behavior in MeOH. Nevertheless, an experiment analogous to the one described before for **16** (shown in Figure 18A on page 41) was performed, adding aq. HCl or aq. NaOH to a solution of **17** in MeOH. Neither of the two additives influenced the absorption or emission spectrum of **17**, emphasizing the very different behavior of these two structurally similar compounds.

### 4.2.3 Fluorescence cell imaging with **16** and **17**

Fluorescence imaging experiments were performed using (healthy) human dermal fibroblast cells (HDF) and melanoma cancer cells (SK-MEL-28). Selected images of stained melanoma cells using **16** or **17** are shown in Figure 23. Compound **16** was distributed all over the cell and mainly visible using the green laser ($\lambda_{ex}$ = 488 nm) for excitation, whereas **17** showed a punctuate pattern and could be imaged using the blue laser ($\lambda_{ex}$ = 405 nm).

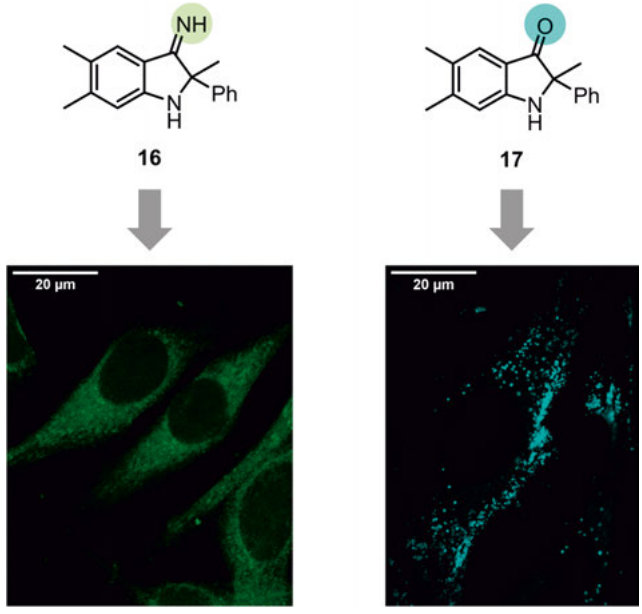


Figure 23. Confocal fluorescence microscopy images of SK-MEL-28 cells stained with **16** or **17** (10 µM, 24 h incubation). Staining was performed on live cells, which were imaged after fixation. Cyan: $\lambda_{ex}$ = 405 nm, green: $\lambda_{ex}$ = 488 nm.

Excitation of compound **16** with the blue laser (instead of the green) resulted in significantly weaker fluorescence (not shown), indicating that the equilibrium between **16** and **16H**$^+$ is shifted towards the protonated (red-shifted) species in the cellular environment. This is in accordance with the expected, based on its p$K_a$ (8.3), as the intracellular pH (p$H_i$) is typically

around 7.2 in normal cells and a little increased in cancer cells.[175] Another observable effect, likely arising from the relatively high p$K_a$ of **16H**$^+$, was the slow partial accumulation of the compound in lysosomes of HDF cells. Figure 24 demonstrates the colocalization of **16** with **Lysotracker Deep Red** (a commercially available lysosome dye) in fibroblast cells. Lysosomes are acidic organelles with pH~5 in normal cells, which is typically slightly decreased in cancer cells (pH~4-5).[176] As mentioned in the general introduction of this thesis (Section 1.4), weakly basic amines such as morpholine can be used as targeting groups for lysosomes. These compounds are typically taken up by lysosomes in their neutral form and are subsequently trapped due to protonation. The p$K_a$ of protonated *N*-alkyl morpholine derivatives is around 7–8[177] (depending on the substituent), which is close to the p$K_a$ of **16H**$^+$. Hence, the acidity of lysosomes is presumably responsible for the accumulation of **16** in this organelle.

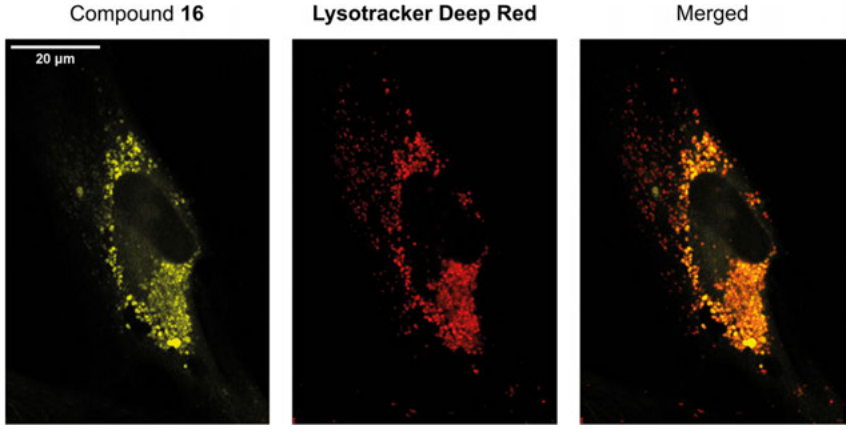


Figure 24. Confocal fluorescence microscopy images of HDF cells showing the colocalization of **16** and lysosomes. After treatment with **16** (20 µM, 24 h incubation), the live cells were co-stained with **Lysotracker Deep Red** (75 nM, 0.5 h) and then imaged after fixation. The image on the left shows **16** (seen in yellow; $\lambda_{ex}$ = 488 nm, $\lambda_{em} \leq$ 600 nm). The image in the middle shows **Lysotracker Deep Red** (seen in red; $\lambda_{ex}$ = 639 nm, $\lambda_{em} \geq$ 640 nm). The image on the right shows the merged images, verifying colocalization.

The lysosomal localization of **16** seemed more specific in the HDF cells than in the SK-MEL-28 cells. This observation was unexpected as the $pH_i$ of cancer cells is usually increased in comparison with normal cells,[175] which should facilitate passive diffusion into the lysosomes as more of neutral **16** should be present in the cytosol. However, since lysosomes are responsible for the degradation of substrates in the cell,[178] the observed distinct staining patterns might be a result of different breakdown efficiencies of **16** by fibroblast and melanoma cell lines.

It should be noted that preliminary studies on additional fibroblast and melanoma cell lines were performed by collaborators specialized on the study of lysosomes. The results indicated that the differences in the staining of HDF and SK-MEL-28 cells with **16** (as described above) were not generally observed with other cell lines, as some melanoma cell lines also indicated partial lysosome staining. The inconsistent lysosomal accumulation was therefore not investigated further.

Initial fluorescence imaging experiments with **17** in melanoma cells showed very rapid photobleaching when images were acquired using the blue channel filter of a widefield fluorescence microscope ($\lambda_{ex}$ = 325–375 nm, $\lambda_{em}$ = 435–485). The bleaching was less pronounced when the cells were imaged using the blue laser of a confocal microscope ($\lambda_{ex}$ = 405 nm). In consequence, it was possible to properly image cells stained with **17** and colocalize the staining pattern with **Nile Red** (a commercially available LD dye, see Section 1.4.2), confirming the accumulation of the fluorophore in lipid droplets (Figure 25).

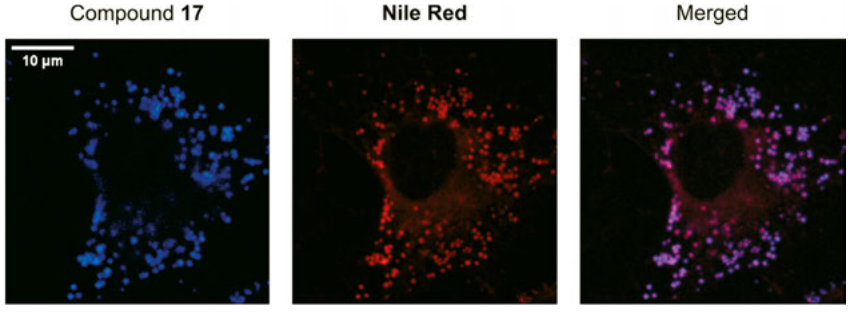


Figure 25. Confocal fluorescence microscopy images of SK-MEL-28 cells showing the colocalization of **17** and LDs. After treatment with **17** (10 µM, 24 h incubation), the cells were fixated and co-stained with **Nile Red** (0.3 µM, 15 min). The image on the left shows **17** (seen in blue; $\lambda_{ex}$ = 405 nm, $\lambda_{em}$ = 420–520 nm). The image in the middle shows **Nile Red** (seen in red; $\lambda_{ex}$ = 555 nm, $\lambda_{em}$ = 570–700 nm). The image on the right shows the merged images, verifying colocalization.

The cell viability of SK-MEL-28 and HDF cells after treatment with **16** or **17** (24 h incubation at 10 or 20 µM) was examined using the Resazurin assay.[138] Both compounds showed no significant cytotoxicity under the studied conditions.

### 4.2.4 Photoisomerization of indolin-3-one **17** in solution

To investigate the fast photobleaching of **17** observed during imaging experiments, the photostability of the fluorophore was examined in a variety of solvents. Equimolar solutions of **17** in apolar solvents (hexane, toluene, and

benzene) exhibited significantly stronger photobleaching than in polar solvents [Acetonitrile (MeCN), DMSO, and MeOH; Figure 26].

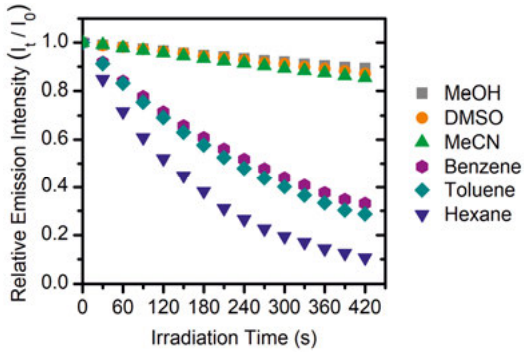


Figure 26. Photobleaching of **17** (25 µM) in various solvents through continuous irradiation in the fluorometer (2.5 mL solution in a 10×10 mm cuvette, $\lambda_{ex}$ / bandwidth = 389 / 20 nm, emission detected around $\lambda_{Emax}$).

The absorption and emission bands of **17** in hexane after irradiation for 420 s, were hypsochromically shifted ($\Delta\lambda_{Amax}$ = 52 nm, $\Delta\lambda_{Emax}$ = 35 nm) compared to the spectra before irradiation, indicating conversion of **17** to a new fluorescent compound (Figure 4C in Paper III). NMR spectroscopy analysis (one- and two-dimensional) of the bleaching product of **17** in hexane (1 h irradiation of 0.8 mM sample solution) revealed that photoisomerization to **18** through ring-opening had occurred (Figure 27).

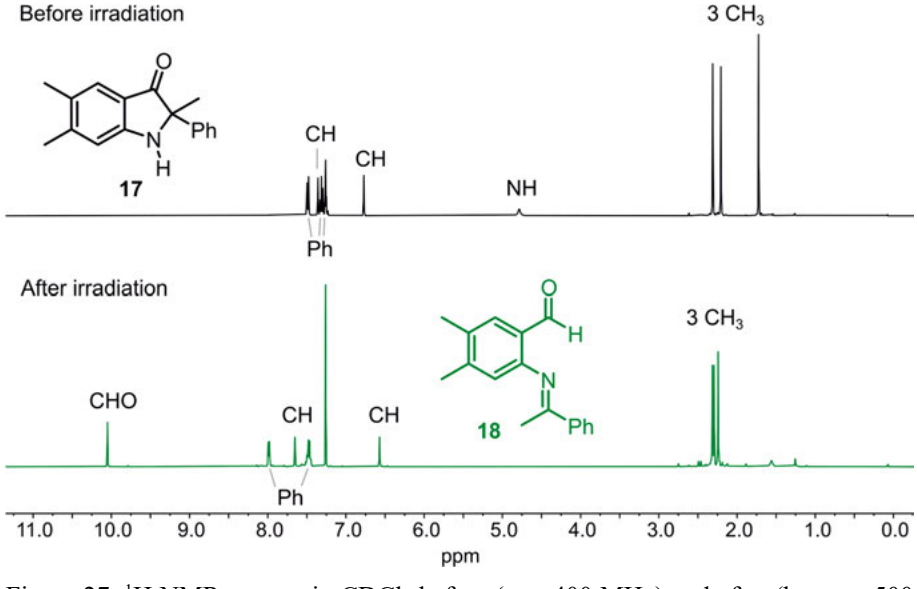


Figure 27. $^1$H NMR spectra in $CDCl_3$ before (top, 400 MHz) and after (bottom, 500 MHz) irradiation of **17** in hexane. The photoconversion product was identified as **18**.

The chemical yield of the photoisomerization reaction was 74%, determined by $^1$H NMR spectroscopy using 1,3,5-trimethoxybenzene as internal standard. The NMR spectrum (Figure 27) indicated full consumption of **17**, with a relatively clean conversion to **18** (traces of unidentified side products were visible). An error margin of around ±5% should be attributed to the chemical yield since the photochemical reaction was performed on a very small scale (0.009 mmol).

Based on classic Norrish radical chemistry, a reaction mechanism for the photoisomerization was proposed (Figure 28). In the following, the proposed mechanism is discussed in two parts, starting with the photophysical aspect and concluding with the radical chemistry of the mechanism.

Upon light irradiation, **17** is elevated to its $S_1$ from which it can either relax to $S_0$, by fluorescence or non-radiatively, or undergo ISC to $T_1$, which is the starting point of the isomerization mechanism. It is known that apolar solvents can facilitate ISC by decreasing the energy gap between singlet and triplet excited states.[179-181] This agrees with the observed increase in the photoconversion rate of **17** in apolar solvents and with the lower fluorescence quantum yield in toluene ($\Phi_F$ = 0.16) compared to DMSO ($\Phi_F$ = 0.41). Furthermore, freeze-pump-thaw degassing of solvents had an accelerating effect on the photoconversion, which might be explained by the lack of quenching of the triplet excited state due to the removal of molecular oxygen. Singlet oxygen generation by **17** upon irradiation was indeed confirmed (in the presence of air) by trapping experiments with 9,10-dimethylanthracene (Figure 5B in Paper III). 9,10-Dimethylanthracene reacts with singlet oxygen to generate the 9,10-endoperoxide, resulting in decreased absorption and emission intensity of the trapping agent.[182]

From the triplet excited state, a radical mechanism was proposed (Figure 28B) consisting of a Norrish type I rearrangement (ring-opening) and Norrish type II hydrogen atom transfer (HAT). The HAT could either occur from the amine or the methyl group. In contrast to HAT from C–H, HAT from N–H is typically dependent on the solvent, with inhibition in polar solvents, which agrees with our experimental observations.[183,184]

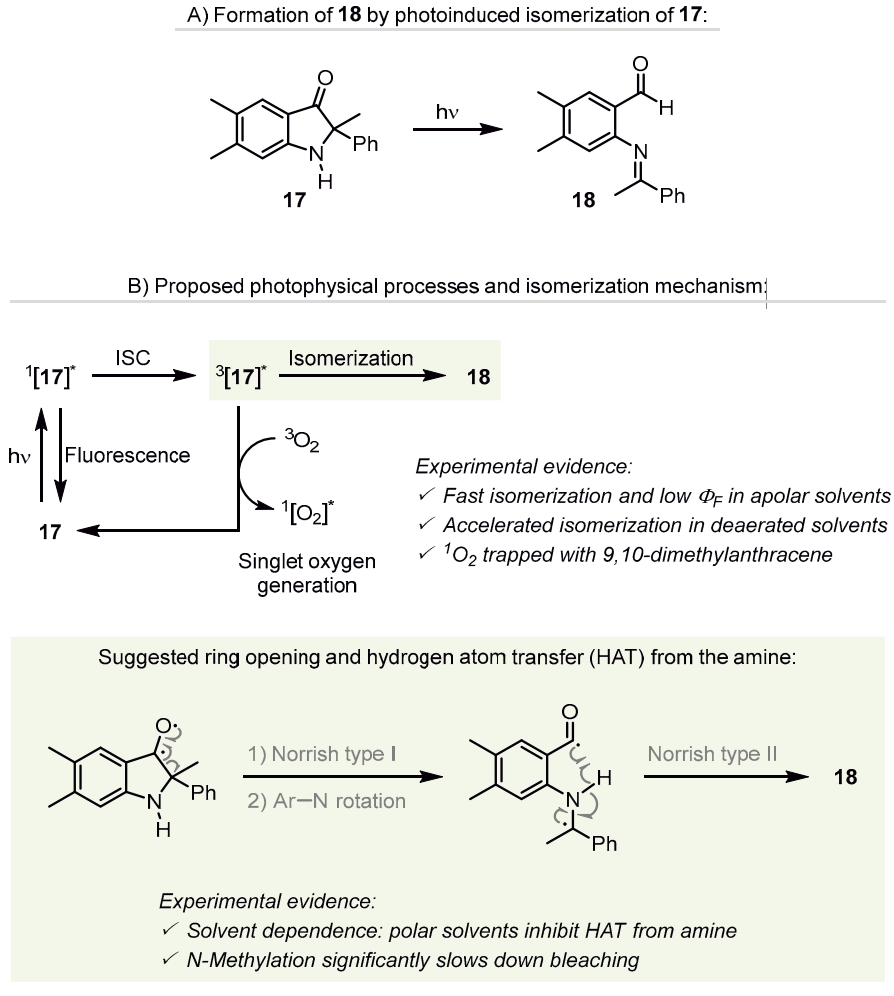


Figure 28. A) Photoisomerization of **17** resulting in **18**. B) Proposed mechanism for the photoisomerization of **17**. Besides isomerization, the triplet excited state ($^3$[**17**]$^*$) can be deactivated by energy transfer to molecular oxygen ($^3O_2$), generating singlet oxygen ($^1O_2$).

To further investigate the mechanism, the *N*-methylated derivative **19** was synthesized (Figure 29A) and its photostability examined. In Figure 29B, the photobleaching behavior of **19** (shown in green) and **17** (shown in purple) are compared in MeOH and hexane. Compound **19** demonstrated high photostability in MeOH and considerably decelerated photobleaching in hexane as compared to **17** (73% and 11% residual emission after 420 s irradiation, respectively). Photooxidative dealkylation is a known process that can affect the photostability of fluorophores containing alkylamines.[30,185] To prevent this molecular oxygen-dependent photoreaction, the irradiation experiment was repeated in deaerated hexane (freeze-pump-thaw method). As

shown in Figure 29B, deaeration had only marginal effects on the results of **19**. On the other hand, in case of **17** the photobleaching was significantly accelerated (as discussed above). NMR spectroscopy analysis of the mixture obtained after irradiation of **19** in deaerated hexane (1 h irradiation of 0.3 mM sample solution) mostly showed **19** and traces of unidentified compounds (not shown). Nevertheless, the higher photostability of **19**, which, in contrast to **17**, does not have a free N–H, supports the proposed photoisomerization mechanism of **17** involving HAT from the amine.

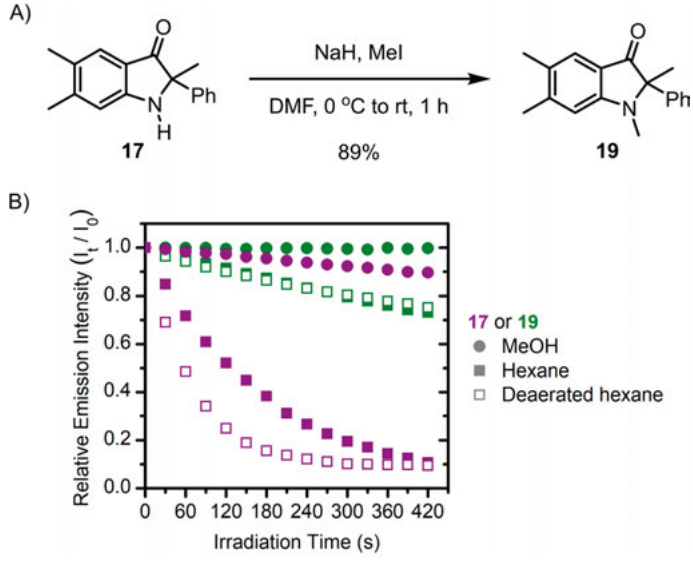


Figure 29. A) Synthesis of **19** through methylation of **17**. B) Photobleaching of **17** (in purple) or **19** (in green) in MeOH (circles), hexane (squares), or deaerated hexane (empty squares). Irradiation was performed in the fluorometer (25 µM, 2.5 mL solution in a 10×10 mm cuvette, $\lambda_{ex}$ / bandwidth = 389 / 20 nm, emission detected around $\lambda_{Emax}$).

In contrast to **17**, indolin-3-imine **16** showed high photostability in polar and apolar solvents under similar conditions (Figure S7 in Paper II Supporting Information). This different photochemical behavior is in accordance with the generally higher reactivity of ketones in photochemical reactions compared to imines.[186,187] Nevertheless, fluorescent pseudoindoxyl derivatives are typically reported with good photostability.[149-151] Although, some photobleaching issues have briefly been mentioned for **LipidGreen2** (see Figure 15 on page 38), though without further elucidation of this observation.[188]

Some of the prevalent photoisomerization reactions investigated in literature are Z/E-photoisomerizations of stilbenes and azobenzenes.[189,190] Furthermore, photoactivated ring-opening reactions have been reported for a few compound classes, such as diarylethenes,[191] spiroheterocycles,[192-194] and

fulgides/fulgimides.[195,196] These compounds are often called photoswitches, as their photoreactions are typically reversible. In contrast, no reversibility of the photoisomerization of the indolin-3-one **17** could be observed.

### 4.2.5 Photoactivated cytotoxicity studies of **17**

To investigate if the photoisomerization process affects the cell viability, SK-MEL-28 cells treated with **17** were exposed to UV light irradiation ($\lambda$ = 365 nm; Figure 30). As a result, the viability was reduced to 63% at 10 µM and to 32% at 20 µM compound concentration after irradiation for 0.5 h. The cell viability was further diminished with longer irradiation time (to 44% at 10 µM, irradiated for 1 h). It should be noted that **17** and **18** without irradiation and the irradiation itself were not cytotoxic. In contrast to normoxic melanoma cells (i.e., 20% $O_2$), irradiation of hypoxic melanoma cells (i.e., 1% $O_2$) treated with **17** did not influence the viability. This result indicates that the oxygen level plays an important role in the photoactivated cytotoxicity of **17**. Considering that singlet oxygen was detected in solution experiments, as described above, it was concluded that the same might occur in cells, which consequently might be responsible for the observed cell death in normoxia. Irradiation experiments with **17** using healthy fibroblast cells gave similar results as for (normoxic) melanoma cells (Figure 30).

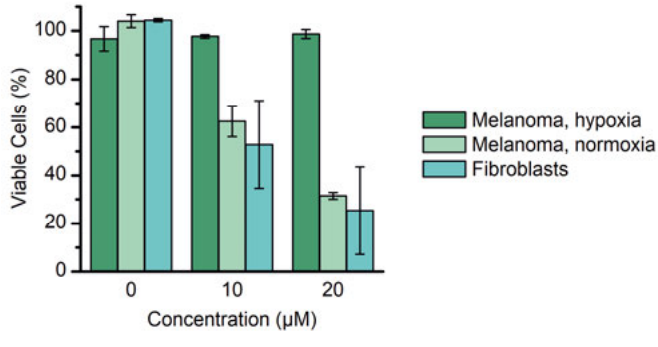


Figure 30. Cell viability of melanoma (dark and light green) and fibroblast (blue) cells treated with **17** (10 or 20 µM, 1 h) compared to DMSO control (i.e., 0 µM of **17**) after irradiation (365 nm, 0.5 h, 1 mW/cm$^2$). The data is presented relative to the corresponding DMSO control as a mean ± standard deviation; n = 2 or 4 (0 and 10 µM, normoxia).

Furthermore, analogous irradiation experiments of normoxic melanoma cells (as described for **17** above) treated with the indolin-3-imine derivative **16** (10 µM) did not indicate photoactivated cytotoxicity (after 0.5 h irradiation).

## 4.3 Summary

The two indoline derivatives (**16** and **17**) studied in Papers II and III are very similar in structure as they only differ by one functional group (imine vs ketone). This simple modification turned a pH sensitive, photobasic, and non-cytotoxic fluorophore that localizes in a polar cellular environment into a light-sensitive and LD-specific fluorophore with photoactivated cytotoxicity (Figure 31).

The indolin-3-imine derivative **16** featured a p$K_a$ of 8.3 in aq. solution and photobasicity with a p$K_a^*$ of approximately 14. The ground and excited state proton transfers were influenced by the acidity of the protic solvent, which affected the absorption and emission spectra, respectively. The compound showed rather unspecific fluorescent cell staining with slow, partial accumulation in lysosomes.

The novel indolin-3-one derivative **17** revealed a unique ability to undergo rapid photoisomerization in apolar solvents. Based on experimental evidence, a radical mechanism involving Norrish type I ring-opening and Norrish type II hydrogen atom transfer was proposed. In the presence of molecular oxygen, singlet oxygen generation was found to be a competing process. This can most likely be related to the observed photoactivated cytotoxicity in normoxic cells.

Overall, the work presented in this Chapter successfully investigated the effect of a small structural modification of an indoline derivative on its photophysical properties and on its utility as a fluorescent probe for cell imaging.

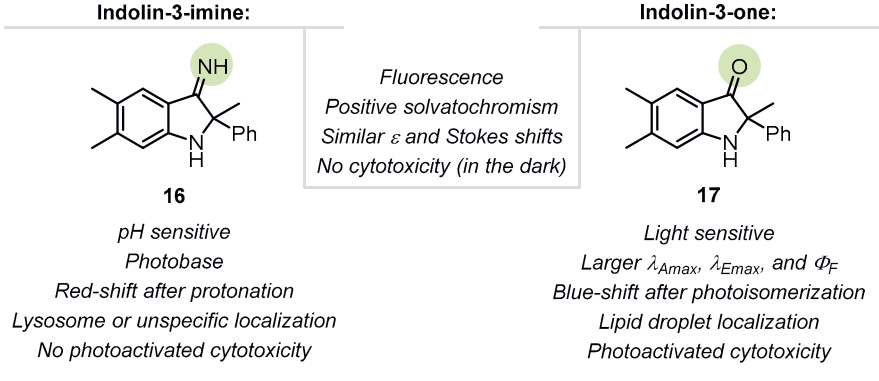


Figure 31. Effect of functional group interconversion of imine and ketone on the photophysical and cellular behavior of indolines **16** and **17**. Mutual properties are presented in the center between the two structures.

# 5 Concluding remarks and future perspectives

This thesis describes the photophysical study of fluorescent 2,1,3-benzothiadiazole and indoline derivatives and their utility as dyes for fluorescence cell microscopy.

All fifteen investigated 4-*N*-substituted BTD derivatives featured large Stokes shifts and fluorescence quenching in polar solvents. The three most lipophilic compounds showed bright and specific staining of LDs in cancer cells (Paper I), indicating that a certain level of lipophilicity is required for accumulation in LDs. The two investigated indoline derivatives, an indolin-3-imine (Paper II) and its ketone analogue (Paper III), demonstrated very different photophysical characteristics and behavior in cells. The indolin-3-imine derivative showed pH sensitivity, with enhanced basicity in the excited state. Furthermore, unspecific staining in melanoma cells and partial staining of lysosomes in fibroblast cells indicated the potential of indolin-3-imine based structures to be applied as fluorescent probes for cell imaging. In contrast, the indolin-3-one derivative exhibited LD-specific cell staining and light-sensitivity due to photoisomerization, along with photoactivated cytotoxicity in normoxic cells.

Future work concerning fluorescent benzothiadiazole and indoline derivatives could focus on further photophysical tuning through structural modifications. Preliminary studies by our group indicate that 5-substituted BTD derivatives, which have largely been overlooked in literature, might be worth exploring. For instance, moving the *para*-dimethylaminophenyl substituent from position 4 to position 5 of BTD, increases the molar extinction coefficient and affects the cell staining result (shows less specific staining). Moreover, new BTD derivatives that retain strong emission in an aq. environment could be developed. Although fluorescence quenching in protic solvents is beneficial for LD staining, compounds without this characteristic could be applied for imaging other intracellular targets or used as general fluorescent tags for biomolecules.

The pH sensitive indolin-3-imine derivative, presented herein, is presumably the first of its kind applied in fluorescence cell imaging and might therefore represent a new class of bioimaging probes. However, further derivatives need to be investigated to verify the general applicability of the indolin-3-imine unit as scaffold for fluorescence cell microscopy. Reducing the basicity, for example by introducing EWGs on the aromatic ring, might

contribute to faster and more specific lysosome accumulation. In addition, an extended study with structurally diverse derivatives could allow for investigating substituent effects on the basicity and the fluorescence quantum yields. An increase of the latter would have a positive impact on the brightness of the fluorophore. The effect of structural variations on the photobasicity could also be investigated to develop probes with large apparent Stokes shifts or new, more efficient (super) photobases.

The indolin-3-one derivative discussed in this thesis is a novel photoisomerizable fluorophore with LD-specific cell staining. To be able to exploit these characteristics in fluorescence cell imaging, future studies could aim at synthetic modifications to inhibit the singlet oxygen generation pathway, which is likely responsible for the photoactivated cytotoxicity. However, structural modifications should also aim at shifting the absorption and emission wavelengths to lower energies (while retaining the photoisomerization ability), so the ring-opened product can clearly be visualized during fluorescence cell microscopy as its precursor. This could yield dual-color photoconvertible fluorophores. Another interesting perspective might concern using this photoisomerization behavior as a new strategy for photoinduced labeling/bioconjugation of intracellular targets through the generated aldehyde or imine moiety. Alternatively, instead of optimizing the properties of this indolin-3-one derivative towards imaging applications, future studies could aim at improving the photoactivated cytotoxicity towards applications in photodynamic therapy. However, that would require red-shifted absorption and emission maxima, which might be achieved with fused aromatic rings. In addition, to enable more efficient singlet oxygen generation, the photoisomerization should be inhibited. For instance, it would be interesting to further investigate the *N*-methylated derivative regarding its singlet oxygen generation efficiency in comparison with the unmethylated structure.

# 6 Sammanfattning på svenska

**Upplysta bensotiadiazoler och indoliner: Fotofysikaliska egenskaper och och avbildning av cancerceller**

Färger kan uppfattas eftersom det finns föreningar som absorberar ljus i det synliga spektrumet. Efter ljusabsorption kan vissa föreningar avge ljus med en längre våglängd (till exempel, rött ljus har längre våglängd än blått ljus). Detta fenomen kallas fluorescens och fluorescerande föreningar kallas fluoroforer. Figur 1 visar hur olika fluoroforer i lösning kan lysa när de bestrålas med ultraviolett ljus.

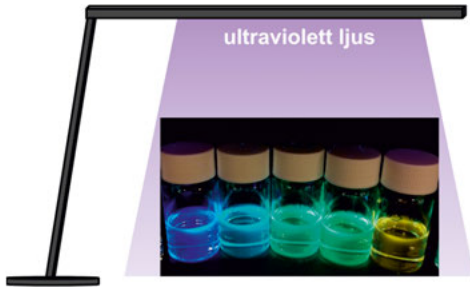


Figur 1. Fluoroforer kan lysa i olika färger när de bestrålas med ljus. Här visas olika fluoroforer i lösning som bestrålas med en lampa som avger ultraviolett ljus. I detta fall så har fluroforerna olika fotofysikaliska egenskaper och därmed är fluorescensen synlig som blått, grönt eller gult ljus.

Fluoroforer spelar en viktig roll inom biovetenskap, till exempel behövs de för att kunna analysera celler med fluorescensmikroskopi. Till skillnad från normal ljusmikroskopi tillåter denna metod specifik avbildning av intracellulära mål, såsom biomolekyler eller organeller. Eftersom många sjukdomar, som cancer, är förknippade med förändringar av intracellulära biologiska processer, är det viktigt att kunna visualisera dessa med hjälp av skräddarsydda prober. Beroende på den specifika forskningsfrågan kan kraven på fluoroforernas egenskaper vara mycket olika. Det finns ingen fluorofor som är perfekt för alla applikationer, vilket gör att kontinuerlig utveckling av nya fluorescerande prober är mycket önskvärt. Under det senaste decenniet har 2,1,3-bensotiadiazolbaserade fluoroforer fått ökad uppmärksamhet, både för applikationer inom organisk elektronik och inom fluorescensavbildning av biologiska prover.

Den första delen av denna avhandling fokuserar på bensotiadiazolbaserade fluoroforer (Figur 2). Femton monosubstituerade bensotiadiazolderivat med amin- eller amidsubstituenter syntetiserades. Deras fotofysikaliska egenskaper studerades först genom absorptions- och fluorescensspektroskopi, i olika lösningsmedel, och sedan testades molekylerna som färgämnen i cancerceller med fluorescensmikroskopi. Aminobensotiadiazolderivaten visade rödförskjuten absorption och fluorescens (d.v.s. längre våglängd) jämfört med de amidsubstituerade derivaten. Energiskillnaden mellan absorptions- och fluorescensmaximum var stor för alla studerade molekyler, vilket är en bra egenskap för användning inom fluorescensmikroskopi. Dessutom visade alla föreningar reducerad fluorescens med ökande lösningsmedelspolaritet. Bara de tre mest lipofila molekylerna i studien (cyklohexylamino-, fenylamino-, och difenylamino-bensotiadiazol) visade ett stark lysande och specifikt färgningsmönster i cancerceller. Vidare analys identifierade färgningsmönstret som ansamling i lipiddroppar. Lipiddroppar är oljiga cellorganeller som är viktiga i energimetabolismen av cancerceller och därför är de betydelsefulla mål inom cancerforskning.

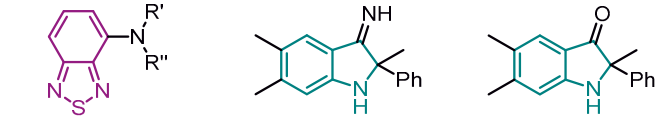


Figur 2. Fluoroforerna som studerades i denna avhandling är baserade på strukturerna bensotiadiazol (lila) och indolin (blågrön). R' och R'' anger olika substituenter.

Den andra delen av denna avhandling fokuserar på indolinbaserade fluorescerande molekyler (Figur 2). Två strukturellt mycket lika derivat, en indolin-3-imin och en indolin-3-on, har undersökts och jämförts med avseende på deras fotofysikaliska egenskaper och användbarhet inom fluorescensmikroskopi av celler. Indolin-3-imin derivatet visade pH-känslighet på grund av dess svagt basiska imingrupp, som blev en starkare bas när den absorberar ljus. Fluorescensmikroskopiexperiment visade ospecifik färgning i melanomceller (hudcancerceller) men benägenhet att ansamlas i lysosomer i fibroblastceller (friska hudceller). Lysosomer är sura organeller vars huvudfunktion är att bryta ner föreningar som inte behövs och vars pH kan bli lite reducerat i cancerceller jämfört med normala celler.

Indolin-3-on derivatet visade ett helt annat beteende. Den visade specifik färgning av lipiddroppar i celler men fluorescensintensiteten minskade snabbt. Detta fotoblekningsbeteende undersöktes sedan spektroskopisk i lösning vilket resulterade i upptäckten av snabb fotoisomerisering av indolin-3-on derivatet genom ringöppning vilket främst sker i opolära lösningsmedel. Ytterligare cellstudier visade att indolin-3-on derivatet också är cytotoxisk när behandlade celler exponeras för bestrålning. En hög fotostabilitet och icke-

cytotoxicitet är dock fördelaktiga egenskaper om fluoroforen ska användas för fluorescensmikroskopi. Därför skulle framtida arbete kunna syfta till att modifiera strukturen så att fotoreaktionen och fototoxiciteten är hämmad.

Sammanfattningsvis bidrar arbetet som presenteras i denna avhandling till utvecklingen av fluoroforer som kan användas i celler och avbildas med fluorescensmikroskopi, som är en viktig metod i forskningen om sjukdomar, till exempel cancer.

# 7 Acknowledgements

First of all, I would like to thank my supervisor *Christine Dyrager*. I am very grateful that you put your faith in me to be your first PhD student. Thank you for all the support and guidance throughout these years and for always keeping a positive mindset.

I am grateful to my co-supervisor *Jan Kihlberg* for supporting me, especially, in challenging situations.

Thank you, *Luke Pilarski*, for encouraging me to pursue a PhD degree and to return to Uppsala to do so.

Thank you, *Helena Grennberg*, for keeping track of my PhD studies and for taking time to provide helpful last-minute feedback for my thesis.

Thank you, *Jan Streuff* and *Chris K.*, for a great collaboration, which resulted in two interesting papers.

Thank you, *Karl* and *Miao*, for keeping the cells happy and for taking time to help me with the experiments. I am also grateful to *Fredrik Swartling* for welcoming me to your laboratories, leading to a very productive collaboration.

Thank you, *Ignacio*, for mentoring my initial computations, which were included in Paper I.

Thank you, *Matt*, *Fredric*, and *Jagadeesh*, for warmly welcoming me back to Uppsala and for all the help when I started my PhD studies. I really enjoyed our discussions about chemistry and life in general. Also, a big thank you to the current members of the Pilarski group, *Fredrik* and *Carolina*, for great discussions and fun joint group activities.

Thank you, *Mauricio*, for being a great colleague and friend throughout these years. Thanks for all the help, especially with NMR spectroscopy and improvising practical solutions to (stupid) problems. I also really appreciated your efforts to cheer me up with cookies, brownies and muffins on the last meters. Thank you!

Thank you, *Susanna*, for all the helpful discussions, your good company in the office and lab, and for giving valuable feedback for my thesis.

Thank you, *Kilian*, for sharing much of your knowledge with me and for a great teamwork in the beginning of my PhD studies.

Thank you, *Hermina*, for answering all my questions about NOESYs and for showing me the Win+L shortcut.

Thank you, *Ivan*, for your great company during late lunches and in general. I am very glad that I can call you my friend.

Thank you, to all past and present members of the Department of Organic Chemistry – BMC for creating such a friendly, respectful, and productive work environment.

Thank you, to all the students that contributed to projects beyond this thesis, who I had the honor to supervise during these years.

I am grateful to *Apotekarsocieteten* for travel grants, giving me the possibility to participate in great conferences.

Danke, *Franzi*, *Eva*, *Nico*, *André*, und *Hummel*, dass ihr seit der Schulzeit meine Freunde geblieben seid und ihr euch immer für mich Zeit nehmt, wenn ich in der Heimat zu Besuch bin. *Franzi*, deine Fische, die meine alten Chemie-Hefte verzieren, haben nun auch ihren Weg in meine Doktorarbeit gefunden.

Tack så mycket, *Markus*, för att du har delat dessa år med mig och för att du påminde mig att det finns mer i livet än bara arbete.

Danke, *Mama*, *Papa*, und *Roland*, für all die unendliche und bedingungslose Unterstützung. *Mama* und *Papa*, ihr habt es mir ermöglicht zu studieren und die erste Doktorin in unserer Familie zu werden. *Roland*, du hast mir ohne zu zögern bei meinen Umzügen nach und in Schweden geholfen, wofür ich sehr dankbar bin, und auch sonst kann ich immer auf deine Hilfe zählen. Dafür bin ich euch unendlich dankbar!

# 8 References


(1) Bray, F.; Laversanne, M.; Weiderpass, E.; Soerjomataram, I. The ever-increasing importance of cancer as a leading cause of premature death worldwide. *Cancer* **2021**, *127* (16), 3029-3030.

(2) Refaat, A.; Yap, M. L.; Pietersz, G.; Walsh, A. P. G.; Zeller, J.; del Rosal, B.; Wang, X.; Peter, K. In vivo fluorescence imaging: success in preclinical imaging paves the way for clinical applications. *J. Nanobiotechnol.* **2022**, *20* (1), 450.

(3) Atkins, P.; de Paula, J. *Atkins' Physical Chemistry*; Oxford University Press Inc., 2002.

(4) Lakowicz, J. R. *Principles of Fluorescence Spectroscopy*; Springer Science+Business Media, LLC, 2006.

(5) Franck, J.; Dymond, E. G. Elementary processes of photochemical reactions. *Trans. Faraday Soc.* **1926**, *21*, 536-542.

(6) Condon, E. U. Nuclear Motions Associated with Electron Transitions in Diatomic Molecules. *Phys. Rev.* **1928**, *32* (6), 858-872.

(7) Jablonski, A. Efficiency of Anti-Stokes Fluorescence in Dyes. *Nature* **1933**, *131*, 839-840.

(8) Kasha, M. Characterization of electronic transitions in complex molecules. *Discuss. Faraday Soc.* **1950**, *9*, 14-19.

(9) Lippert, E. Dipolmoment und Elektronenstruktur von angeregten Molekülen. *Z. Naturforsch. A* **1955**, *10* (7), 541-545.

(10) Mataga, N.; Kaifu, Y.; Koizumi, M. Solvent Effects upon Fluorescence Spectra and the Dipolemoments of Excited Molecules. *Bull. Chem. Soc. Jpn.* **1956**, *29* (4), 465-470.

(11) Grabowski, Z. R.; Rotkiewicz, K.; Rettig, W. Structural Changes Accompanying Intramolecular Electron Transfer: Focus on Twisted Intramolecular Charge-Transfer States and Structures. *Chem. Rev.* **2003**, *103* (10), 3899-4032.

(12) Kumpulainen, T.; Lang, B.; Rosspeintner, A.; Vauthey, E. Ultrafast Elementary Photochemical Processes of Organic Molecules in Liquid Solution. *Chem. Rev.* **2017**, *117* (16), 10826-10939.

(13) Würth, C.; Grabolle, M.; Pauli, J.; Spieles, M.; Resch-Genger, U. Relative and absolute determination of fluorescence quantum yields of transparent samples. *Nat. Protoc.* **2013**, *8* (8), 1535-1550.

(14) Brouwer, A. M. Standards for photoluminescence quantum yield measurements in solution (IUPAC Technical Report). *Pure Appl. Chem.* **2011**, *83* (12), 2213-2228.

(15) Sjöback, R.; Nygren, J.; Kubista, M. Absorption and fluorescence properties of fluorescein. *Spectrochim. Acta, Part A* **1995**, *51* (6), L7-L21.

(16) NobelPrize.org. Nobel Prize Outreach AB 2023. *The Nobel Prize in Chemistry 2014*. https://www.nobelprize.org/prizes/chemistry/2014/summary/ (accessed 9 June 2023).

(17) Lichtman, J. W.; Conchello, J.-A. Fluorescence microscopy. *Nat. Methods* **2005**, *2* (12), 910-919.
(18) Murphy, D. B.; Davidson, M. W. Confocal Laser Scanning Microscopy. In *Fundamentals of Light Microscopy and Electronic Imaging*, 2nd ed.; John Wiley & Sons, Inc., 2012; pp 265-305.
(19) Lavis, L. D.; Raines, R. T. Bright Ideas for Chemical Biology. *ACS Chem. Biol.* **2008**, *3* (3), 142-155.
(20) Lavis, L. D.; Raines, R. T. Bright Building Blocks for Chemical Biology. *ACS Chem. Biol.* **2014**, *9* (4), 855-866.
(21) Grimm, J. B.; Lavis, L. D. Caveat fluorophore: an insiders' guide to small-molecule fluorescent labels. *Nat. Methods* **2022**, *19* (2), 149-158.
(22) Colas, K.; Doloczki, S.; Posada Urrutia, M.; Dyrager, C. Prevalent Bioimaging Scaffolds: Synthesis, Photophysical Properties and Applications. *Eur. J. Org. Chem.* **2021**, *2021* (15), 2133-2144.
(23) Burry, R. W. *Immunocytochemistry: A Practical Guide for Biomedical Research*; Springer New York, NY, 2010.
(24) Martínek, M.; Ludvíková, L.; Šranková, M.; Navrátil, R.; Muchová, L.; Huzlík, J.; Vítek, L.; Klán, P.; Šebej, P. Common xanthene fluorescent dyes are visible-light activatable CO-releasing molecules. *Org. Biomol. Chem.* **2023**, *21* (1), 93-97.
(25) Nani, R. R.; Kelley, J. A.; Ivanic, J.; Schnermann, M. J. Reactive species involved in the regioselective photooxidation of heptamethine cyanines. *Chem. Sci.* **2015**, *6* (11), 6556-6563.
(26) Matikonda, S. S.; Helmerich, D. A.; Meub, M.; Beliu, G.; Kollmannsberger, P.; Greer, A.; Sauer, M.; Schnermann, M. J. Defining the Basis of Cyanine Phototruncation Enables a New Approach to Single-Molecule Localization Microscopy. *ACS Cent. Sci.* **2021**, *7* (7), 1144-1155.
(27) Loudet, A.; Burgess, K. BODIPY Dyes and Their Derivatives: Syntheses and Spectroscopic Properties. *Chem. Rev.* **2007**, *107* (11), 4891-4932.
(28) Ren, T.-B.; Xu, W.; Zhang, W.; Zhang, X.-X.; Wang, Z.-Y.; Xiang, Z.; Yuan, L.; Zhang, X.-B. A General Method To Increase Stokes Shift by Introducing Alternating Vibronic Structures. *J. Am. Chem. Soc.* **2018**, *140* (24), 7716-7722.
(29) Jiang, G.; Ren, T.-B.; D'Este, E.; Xiong, M.; Xiong, B.; Johnsson, K.; Zhang, X.-B.; Wang, L.; Yuan, L. A synergistic strategy to develop photostable and bright dyes with long Stokes shift for nanoscopy. *Nat Commun* **2022**, *13* (1), 2264.
(30) Butkevich, A. N.; Bossi, M. L.; Lukinavičius, G.; Hell, S. W. Triarylmethane Fluorophores Resistant to Oxidative Photobluing. *J. Am. Chem. Soc.* **2019**, *141* (2), 981-989.
(31) Zheng, Q.; Lavis, L. D. Development of photostable fluorophores for molecular imaging. *Curr. Opin. Chem. Biol.* **2017**, *39*, 32-38.
(32) Altman, R. B.; Terry, D. S.; Zhou, Z.; Zheng, Q.; Geggier, P.; Kolster, R. A.; Zhao, Y.; Javitch, J. A.; Warren, J. D.; Blanchard, S. C. Cyanine fluorophore derivatives with enhanced photostability. *Nat. Methods* **2012**, *9* (1), 68-71.
(33) Schwechheimer, C.; Rönicke, F.; Schepers, U.; Wagenknecht, H.-A. A new structure–activity relationship for cyanine dyes to improve photostability and fluorescence properties for live cell imaging. *Chem. Sci.* **2018**, *9* (31), 6557-6563.
(34) Štacková, L.; Muchová, E.; Russo, M.; Slavíček, P.; Štacko, P.; Klán, P. Deciphering the Structure–Property Relations in Substituted Heptamethine Cyanines. *J. Org. Chem.* **2020**, *85* (15), 9776-9790.

(35) Yang, J.; Wang, K.; Zheng, Y.; Piao, Y.; Wang, J.; Tang, J.; Shen, Y.; Zhou, Z. Molecularly Precise, Bright, Photostable, and Biocompatible Cyanine Nanodots as Alternatives to Quantum Dots for Biomedical Applications. *Angew. Chem. Int. Ed.* **2022**, *61* (36), e202202128.
(36) Wan, C.-W.; Burghart, A.; Chen, J.; Bergström, F.; Johansson, L. B.-Å.; Wolford, M. F.; Kim, T. G.; Topp, M. R.; Hochstrasser, R. M.; Burgess, K. Anthracene–BODIPY Cassettes: Syntheses and Energy Transfer. *Chem. Eur. J.* **2003**, *9* (18), 4430-4441.
(37) Ziessel, R.; Goze, C.; Ulrich, G.; Césario, M.; Retailleau, P.; Harriman, A.; Rostron, J. P. Intramolecular Energy Transfer in Pyrene–Bodipy Molecular Dyads and Triads. *Chem. Eur. J.* **2005**, *11* (24), 7366-7378.
(38) Ulrich, G.; Ziessel, R.; Harriman, A. The Chemistry of Fluorescent Bodipy Dyes: Versatility Unsurpassed. *Angew. Chem. Int. Ed.* **2008**, *47* (7), 1184-1201.
(39) Bittel, A. M.; Davis, A. M.; Wang, L.; Nederlof, M. A.; Escobedo, J. O.; Strongin, R. M.; Gibbs, S. L. Varied Length Stokes Shift BODIPY-Based Fluorophores for Multicolor Microscopy. *Sci. Rep.* **2018**, *8* (1), 4590.
(40) Schäfer, C.; Mony, J.; Olsson, T.; Börjesson, K. Effect of the Aza-N-Bridge and Push–Pull Moieties: A Comparative Study between BODIPYs and Aza-BODIPYs. *J. Org. Chem.* **2022**, *87* (5), 2569-2579.
(41) Burghart, A.; Kim, H.; Welch, M. B.; Thoresen, L. H.; Reibenspies, J.; Burgess, K.; Bergström, F.; Johansson, L. B. Å. 3,5-Diaryl-4,4-difluoro-4-bora-3a,4a-diaza-s-indacene (BODIPY) Dyes: Synthesis, Spectroscopic, Electrochemical, and Structural Properties. *J. Org. Chem.* **1999**, *64* (21), 7813-7819.
(42) Michie, M. S.; Götz, R.; Franke, C.; Bowler, M.; Kumari, N.; Magidson, V.; Levitus, M.; Loncarek, J.; Sauer, M.; Schnermann, M. J. Cyanine Conformational Restraint in the Far-Red Range. *J. Am. Chem. Soc.* **2017**, *139* (36), 12406-12409.
(43) Grimm, J. B.; English, B. P.; Chen, J.; Slaughter, J. P.; Zhang, Z.; Revyakin, A.; Patel, R.; Macklin, J. J.; Normanno, D.; Singer, R. H.; Lionnet, T.; Lavis, L. D. A general method to improve fluorophores for live-cell and single-molecule microscopy. *Nat. Methods* **2015**, *12* (3), 244-250.
(44) Kim, E.; Koh, M.; Ryu, J.; Park, S. B. Combinatorial Discovery of Full-Color-Tunable Emissive Fluorescent Probes Using a Single Core Skeleton, 1,2-Dihydropyrrolo[3,4-β]indolizin-3-one. *J. Am. Chem. Soc.* **2008**, *130* (37), 12206-12207.
(45) Kim, E.; Koh, M.; Lim, B. J.; Park, S. B. Emission Wavelength Prediction of a Full-Color-Tunable Fluorescent Core Skeleton, 9-Aryl-1,2-dihydropyrrolo[3,4-b]indolizin-3-one. *J. Am. Chem. Soc.* **2011**, *133* (17), 6642-6649.
(46) Kim, T.; Kim, J. Color-Tunable Indolizine-Based Fluorophores and Fluorescent pH Sensor. *Molecules* **2022**, *27* (1), 12.
(47) Kim, E.; Lee, Y.; Lee, S.; Park, S. B. Discovery, Understanding, and Bioapplication of Organic Fluorophore: A Case Study with an Indolizine-Based Novel Fluorophore, Seoul-Fluor. *Acc. Chem. Res.* **2015**, *48* (3), 538-547.
(48) Wang, S.; Shi, H.; Wang, L.; Loredo, A.; Bachilo, S. M.; Wu, W.; Tian, Z.; Chen, Y.; Weisman, R. B.; Zhang, X.; Cheng, Z.; Xiao, H. Photostable Small-Molecule NIR-II Fluorescent Scaffolds that Cross the Blood–Brain Barrier for Noninvasive Brain Imaging. *J. Am. Chem. Soc.* **2022**, *144* (51), 23668-23676.

(49) Chang, M. C.; Chantzis, A.; Jacquemin, D.; Otten, E. Boron difluorides with formazanate ligands: redox-switchable fluorescent dyes with large stokes shifts. *Dalton Trans.* **2016**, *45* (23), 9477-9484.
(50) Maar, R. R.; Barbon, S. M.; Sharma, N.; Groom, H.; Luyt, L. G.; Gilroy, J. B. Evaluation of Anisole-Substituted Boron Difluoride Formazanate Complexes for Fluorescence Cell Imaging. *Chem. Eur. J.* **2015**, *21* (44), 15589-15599.
(51) Barbon, S. M.; Novoa, S.; Bender, D.; Groom, H.; Luyt, L. G.; Gilroy, J. B. Copper-assisted azide–alkyne cycloaddition chemistry as a tool for the production of emissive boron difluoride 3-cyanoformazanates. *Org. Chem. Front.* **2017**, *4* (2), 178-190.
(52) Fu, M.; Xiao, Y.; Qian, X.; Zhao, D.; Xu, Y. A design concept of long-wavelength fluorescent analogs of rhodamine dyes: replacement of oxygen with silicon atom. *Chem. Commun.* **2008**, (15), 1780-1782.
(53) Koide, Y.; Urano, Y.; Hanaoka, K.; Terai, T.; Nagano, T. Evolution of Group 14 Rhodamines as Platforms for Near-Infrared Fluorescence Probes Utilizing Photoinduced Electron Transfer. *ACS Chem. Biol.* **2011**, *6* (6), 600-608.
(54) Lukinavičius, G.; Reymond, L.; Umezawa, K.; Sallin, O.; D'Este, E.; Göttfert, F.; Ta, H.; Hell, S. W.; Urano, Y.; Johnsson, K. Fluorogenic Probes for Multicolor Imaging in Living Cells. *J. Am. Chem. Soc.* **2016**, *138* (30), 9365-9368.
(55) Lukinavičius, G.; Umezawa, K.; Olivier, N.; Honigmann, A.; Yang, G.; Plass, T.; Mueller, V.; Reymond, L.; Corrêa Jr, I. R.; Luo, Z.-G.; Schultz, C.; Lemke, E. A.; Heppenstall, P.; Eggeling, C.; Manley, S.; Johnsson, K. A near-infrared fluorophore for live-cell super-resolution microscopy of cellular proteins. *Nature Chem* **2013**, *5* (2), 132-139.
(56) Ikeno, T.; Nagano, T.; Hanaoka, K. Silicon-substituted Xanthene Dyes and Their Unique Photophysical Properties for Fluorescent Probes. *Chem. Asian J.* **2017**, *12* (13), 1435-1446.
(57) Kushida, Y.; Nagano, T.; Hanaoka, K. Silicon-substituted xanthene dyes and their applications in bioimaging. *Analyst* **2015**, *140* (3), 685-695.
(58) Oliveira, F. F.; Santos, D. C.; Lapis, A. A.; Correa, J. R.; Gomes, A. F.; Gozzo, F. C.; Moreira, P. F., Jr.; de Oliveira, V. C.; Quina, F. H.; Neto, B. A. On the use of 2,1,3-benzothiadiazole derivatives as selective live cell fluorescence imaging probes. *Bioorg. Med. Chem. Lett.* **2010**, *20* (20), 6001-6007.
(59) Carvalho, P. H. P. R.; Correa, J. R.; Guido, B. C.; Gatto, C. C.; De Oliveira, H. C. B.; Soares, T. A.; Neto, B. A. D. Designed Benzothiadiazole Fluorophores for Selective Mitochondrial Imaging and Dynamics. *Chem. Eur. J.* **2014**, *20* (47), 15360-15374.
(60) Mota, A. A. R.; Carvalho, P. H. P. R.; Guido, B. C.; de Oliveira, H. C. B.; Soares, T. A.; Corrêa, J. R.; Neto, B. A. D. Bioimaging, cellular uptake and dynamics in living cells of a lipophilic fluorescent benzothiadiazole at low temperature (4 °C). *Chem. Sci.* **2014**, *5* (10), 3995-4003.
(61) Neto, B. A. D.; Correa, J. R.; Spencer, J. Fluorescent Benzothiadiazole Derivatives as Fluorescence Imaging Dyes: A Decade of New Generation Probes. *Chem. Eur. J.* **2022**, *28* (4), e202103262.
(62) Wang, L.; Frei, M. S.; Salim, A.; Johnsson, K. Small-Molecule Fluorescent Probes for Live-Cell Super-Resolution Microscopy. *J. Am. Chem. Soc.* **2019**, *141* (7), 2770-2781.
(63) Collot, M.; Fam, T. K.; Ashokkumar, P.; Faklaris, O.; Galli, T.; Danglot, L.; Klymchenko, A. S. Ultrabright and Fluorogenic Probes for Multicolor Imaging and Tracking of Lipid Droplets in Cells and Tissues. *J. Am. Chem. Soc.* **2018**, *140* (16), 5401-5411.

(64) Danylchuk, D. I.; Jouard, P. H.; Klymchenko, A. S. Targeted Solvatochromic Fluorescent Probes for Imaging Lipid Order in Organelles under Oxidative and Mechanical Stress. *J. Am. Chem. Soc.* **2021**, *143* (2), 912-924.
(65) Zhu, H.; Fan, J.; Du, J.; Peng, X. Fluorescent Probes for Sensing and Imaging within Specific Cellular Organelles. *Acc. Chem. Res.* **2016**, *49* (10), 2115-2126.
(66) Choi, N.-E.; Lee, J.-Y.; Park, E.-C.; Lee, J.-H.; Lee, J. Recent Advances in Organelle-Targeted Fluorescent Probes. *Molecules* **2021**, *26* (1), 217.
(67) Hou, J.-T.; Ren, W. X.; Li, K.; Seo, J.; Sharma, A.; Yu, X.-Q.; Kim, J. S. Fluorescent bioimaging of pH: from design to applications. *Chem. Soc. Rev.* **2017**, *46* (8), 2076-2090.
(68) Yin, J.; Huang, L.; Wu, L.; Li, J.; James, T. D.; Lin, W. Small molecule based fluorescent chemosensors for imaging the microenvironment within specific cellular regions. *Chem. Soc. Rev.* **2021**, *50* (21), 12098-12150.
(69) Zielonka, J.; Joseph, J.; Sikora, A.; Hardy, M.; Ouari, O.; Vasquez-Vivar, J.; Cheng, G.; Lopez, M.; Kalyanaraman, B. Mitochondria-Targeted Triphenylphosphonium-Based Compounds: Syntheses, Mechanisms of Action, and Therapeutic and Diagnostic Applications. *Chem. Rev.* **2017**, *117* (15), 10043-10120.
(70) Chen, H.; Yu, Z.; Ren, S.; Qiu, Y. Fluorescent Probes Design Strategies for Imaging Mitochondria and Lysosomes. *Front. Pharmacol.* **2022**, *13*, 915609.
(71) Fam, T. K.; Klymchenko, A. S.; Collot, M. Recent Advances in Fluorescent Probes for Lipid Droplets. *Materials* **2018**, *11* (9), 1768.
(72) Zhao, Y.; Shi, W.; Li, X.; Ma, H. Recent advances in fluorescent probes for lipid droplets. *Chem. Commun.* **2022**, *58* (10), 1495-1509.
(73) Olzmann, J. A.; Carvalho, P. Dynamics and functions of lipid droplets. *Nat. Rev. Mol. Cell Biol.* **2019**, *20* (3), 137-155.
(74) Li, Z.; Liu, H.; Luo, X. Lipid droplet and its implication in cancer progression. *Am. J. Cancer Res.* **2020**, *10* (12), 4112-4122.
(75) Cruz, A. L. S.; Barreto, E. d. A.; Fazolini, N. P. B.; Viola, J. P. B.; Bozza, P. T. Lipid droplets: platforms with multiple functions in cancer hallmarks. *Cell Death Dis.* **2020**, *11* (2), 105.
(76) Shyu, P., Jr; Wong, X. F. A.; Crasta, K.; Thibault, G. Dropping in on lipid droplets: insights into cellular stress and cancer. *Biosci. Rep.* **2018**, *38* (5).
(77) Pellerin, L.; Carrié, L.; Dufau, C.; Nieto, L.; Ségui, B.; Levade, T.; Riond, J.; Andrieu-Abadie, N. Lipid metabolic Reprogramming: Role in Melanoma Progression and Therapeutic Perspectives. *Cancers* **2020**, *12* (11), 3147.
(78) Huang, D.; Li, C.; Zhang, H. Hypoxia and cancer cell metabolism. *Acta Biochim. Biophys. Sin.* **2014**, *46* (3), 214-219.
(79) Petrova, V.; Annicchiarico-Petruzzelli, M.; Melino, G.; Amelio, I. The hypoxic tumour microenvironment. *Oncogenesis* **2018**, *7* (1), 10.
(80) Challapalli, A.; Carroll, L.; Aboagye, E. O. Molecular mechanisms of hypoxia in cancer. *Clin. Transl. Imaging* **2017**, *5* (3), 225-253.
(81) Hypoxia/Normoxia. Hypoxia/Normoxia. In *Encyclopedic Reference of Genomics and Proteomics in Molecular Medicine*, Springer, 2006.
(82) Greenspan, P.; Mayer, E. P.; Fowler, S. D. Nile red: a selective fluorescent stain for intracellular lipid droplets. *J. Cell Biol.* **1985**, *100* (3), 965-973.
(83) Gocze, P. M.; Freeman, D. A. Factors underlying the variability of lipid droplet fluorescence in MA-10 leydig tumor cells. *Cytometry* **1994**, *17* (2), 151-158.
(84) Thermo Fisher Scientific Inc. *BODIPY™ 493/503 (4,4-Difluoro-1,3,5,7,8-Pentamethyl-4-Bora-3a,4a-Diaza-s-Indacene)*. https://www.thermofisher.com/order/catalog/product/D3922 (accessed 16 March 2021).

(85) Koopman, R.; Schaart, G.; Hesselink, M. K. Optimisation of oil red O staining permits combination with immunofluorescence and automated quantification of lipids. *Histochem. Cell Biol.* **2001**, *116* (1), 63-68.
(86) Listenberger, L. L.; Studer, A. M.; Brown, D. A.; Wolins, N. E. Fluorescent Detection of Lipid Droplets and Associated Proteins. *Curr. Protoc. Cell Biol.* **2016**, *71* (1), 4.31.1-4.31.14.
(87) Fukumoto, S.; Fujimoto, T. Deformation of lipid droplets in fixed samples. *Histochem. Cell Biol.* **2002**, *118* (5), 423-428.
(88) Tian, H.; Sedgwick, A. C.; Han, H.-H.; Sen, S.; Chen, G.-R.; Zang, Y.; Sessler, J. L.; James, T. D.; Li, J.; He, X.-P. Fluorescent probes for the imaging of lipid droplets in live cells. *Coord. Chem. Rev.* **2021**, *427*, 213577.
(89) Miranda, M. S.; Matos, M. A. R.; Morais, V. M. F.; Liebman, J. F. 2,1,3-Benzothiadiazole: Study of its structure, energetics and aromaticity. *J. Chem. Thermodyn.* **2012**, *50*, 30-36.
(90) Wang, Y.; Michinobu, T. Benzothiadiazole and its π-extended, heteroannulated derivatives: useful acceptor building blocks for high-performance donor–acceptor polymers in organic electronics. *J. Mater. Chem. C* **2016**, *4* (26), 6200-6214.
(91) Neto, B. A. D.; Lapis, A. A. M.; da Silva Júnior, E. N.; Dupont, J. 2,1,3-Benzothiadiazole and Derivatives: Synthesis, Properties, Reactions, and Applications in Light Technology of Small Molecules. *Eur. J. Org. Chem.* **2013**, *2013* (2), 228-255.
(92) Du, J.; Biewer, M. C.; Stefan, M. C. Benzothiadiazole building units in solution-processable small molecules for organic photovoltaics. *J. Mater. Chem. A* **2016**, *4* (41), 15771-15787.
(93) Wu, Y.; Zhu, W. Organic sensitizers from D–π–A to D–A–π–A: effect of the internal electron-withdrawing units on molecular absorption, energy levels and photovoltaic performances. *Chem. Soc. Rev.* **2013**, *42* (5), 2039-2058.
(94) Neto, B. A. D.; Carvalho, P. H. P. R.; Correa, J. R. Benzothiadiazole Derivatives as Fluorescence Imaging Probes: Beyond Classical Scaffolds. *Acc. Chem. Res.* **2015**, *48* (6), 1560-1569.
(95) Gu, H.; Liu, W.; Li, H.; Sun, W.; Du, J.; Fan, J.; Peng, X. 2,1,3-Benzothiadiazole derivative AIEgens for smart phototheranostics. *Coord. Chem. Rev.* **2022**, *473*, 214803.
(96) Li, L.; Xiong, Z.; Dang, Y.; Li, Y.; Zhang, A.; Ding, C.; Xu, Z.; Zhang, W. A red-emissive D-A-D type fluorescent probe for lysosomal pH imaging. *Anal Methods* **2020**, *12* (23), 2978-2984.
(97) Rakitin, O. A. Recent Developments in the Synthesis of 1,2,5-Thiadiazoles and 2,1,3-Benzothiadiazoles. *Synthesis* **2019**, *51* (23), 4338-4347.
(98) Pilgram, K.; Zupan, M.; Skiles, R. Bromination of 2,1,3-benzothiadiazoles. *J. Heterocycl. Chem.* **1970**, *7* (3), 629-633.
(99) Thooft, A. M.; Cassaidy, K.; VanVeller, B. A Small Push-Pull Fluorophore for Turn-on Fluorescence. *J. Org. Chem.* **2017**, *82* (17), 8842-8847.
(100) Uchiyama, S.; Kimura, K.; Gota, C.; Okabe, K.; Kawamoto, K.; Inada, N.; Yoshihara, T.; Tobita, S. Environment-sensitive fluorophores with benzothiadiazole and benzoselenadiazole structures as candidate components of a fluorescent polymeric thermometer. *Chem. Eur. J.* **2012**, *18* (31), 9552-9563.
(101) Kawamoto, K.; Uchiyama, S. New Fluorogenic Benzothiadiazole and Benzoselenadiazole Reagents to Yield Environment-sensitive Fluorophores via a Reaction with Amines. *Chem. Lett.* **2012**, *41* (11), 1451-1452.

(102) Sakurai, H.; Ritonga, M. T.; Shibatani, H.; Hirao, T. Synthesis and characterization of p-phenylenediamine derivatives bearing an electron-acceptor unit. *J. Org. Chem.* **2005**, *70* (7), 2754-2762.
(103) Han, X.; Gong, W.; Tong, Y.; Wei, D.; Wang, Y.; Ding, J.; Hou, H.; Song, Y. Synthesis and properties of benzothiadiazole-pyridine system: The modulation of optical feature. *Dyes Pigm.* **2017**, *137*, 135-142.
(104) Sukhikh, T. S.; Khisamov, R. M.; Bashirov, D. A.; Kovtunova, L. M.; Kuratieva, N. V.; Konchenko, S. N. Substituent Effect on the Structure and Photophysical Properties of Phenylamino- and Pyridylamino-2,1,3-Benzothiadiazoles. *J. Struct. Chem.* **2019**, *60* (10), 1670-1680.
(105) Zhang, J.; Parker, T. C.; Chen, W.; Williams, L.; Khrustalev, V. N.; Jucov, E. V.; Barlow, S.; Timofeeva, T. V.; Marder, S. R. C–H-Activated Direct Arylation of Strong Benzothiadiazole and Quinoxaline-Based Electron Acceptors. *J. Org. Chem.* **2016**, *81* (2), 360-370.
(106) Zhang, J.; Chen, W.; Rojas, A. J.; Jucov, E. V.; Timofeeva, T. V.; Parker, T. C.; Barlow, S.; Marder, S. R. Controllable Direct Arylation: Fast Route to Symmetrical and Unsymmetrical 4,7-Diaryl-5,6-difluoro-2,1,3-benzothiadiazole Derivatives for Organic Optoelectronic Materials. *J. Am. Chem. Soc.* **2013**, *135* (44), 16376-16379.
(107) He, C.-Y.; Wu, C.-Z.; Qing, F.-L.; Zhang, X. Direct (Het)Arylation of Fluorinated Benzothiadiazoles and Benzotriazole with (Het)Aryl Iodides. *J. Org. Chem.* **2014**, *79* (4), 1712-1718.
(108) Idris, I.; Tannoux, T.; Derridj, F.; Dorcet, V.; Boixel, J.; Guerchais, V.; Soulé, J.-F.; Doucet, H. Effective modulation of the photoluminescence properties of 2,1,3-benzothiadiazoles and 2,1,3-benzoselenadiazoles by Pd-catalyzed C–H bond arylations. *J. Mater. Chem. C* **2018**, *6* (7), 1731-1737.
(109) Zimdars, S.; Langhals, H.; Knochel, P. Functionalization of the Benzo[c][1,2,5]thiadiazole Scaffold via Mg-, Zn- and Mn-Intermediates. *Synthesis* **2011**, *2011* (08), 1302-1308.
(110) Shome, S.; Singh, S. P. Access to small molecule semiconductors via C–H activation for photovoltaic applications. *Chem. Commun.* **2018**, *54* (53), 7322-7325.
(111) Murugesh, V.; Reddy, P. R.; Singh, S. P. Photocatalyst-free visible-light triggered amination of benzo[c][1,2,5]thiadiazole: direct C–N bond formation from C(sp2)–H bond. *Chem. Commun.* **2023**, *59* (8), 1034-1037.
(112) He, H.; Guo, J.; Sun, W.; Yang, B.; Zhang, F.; Liang, G. Palladium-Catalyzed Direct Mono- or Polyhalogenation of Benzothiadiazole Derivatives. *J. Org. Chem.* **2020**, *85* (5), 3788-3798.
(113) Guo, J.; He, H.; Ye, Z.; Zhu, K.; Wu, Y.; Zhang, F. Highly Selective Palladium-Catalyzed Arene C–H Acyloxylation with Benzothiadiazole as a Modifiable Directing Group. *Org. Lett.* **2018**, *20* (18), 5692-5695.
(114) Reddy, C.; Bisht, N.; Parella, R.; Babu, S. A. 4-Amino-2,1,3-benzothiadiazole as a Removable Bidentate Directing Group for the Pd(II)-Catalyzed Arylation/Oxygenation of sp2/sp3 β-C–H Bonds of Carboxamides. *J. Org. Chem.* **2016**, *81* (24), 12143-12168.
(115) Bisht, N.; Arulananda Babu, S.; Tomar, R. Utility of 4-Amino-2,1,3-benzothiadiazole Directing Group in the Pd(II)-catalyzed Arylation of γ-C−H Bonds of Carboxamides and β-C-H Bonds of Amino Acid Carboxamides. *Asian J. Org. Chem.* **2022**, *11* (12), e202200589.

(116) Shigehiro, T.; Yagi, S.; Maeda, T.; Nakazumi, H.; Fujiwara, H.; Sakurai, Y. Novel 10,13-disubstituted dipyrido[3,2-a:2′,3′-c]phenazines and their platinum(II) complexes: highly luminescent ICT-type fluorophores based on D–A–D structures. *Tetrahedron Lett.* **2014**, *55* (37), 5195-5198.
(117) Prashad, M.; Liu, Y.; Repič, O. A practical method for the reduction of 2,1,3-benzothiadiazoles to 1,2-benzenediamines with magnesium and methanol. *Tetrahedron Lett.* **2001**, *42* (12), 2277-2279.
(118) Tsubata, Y.; Suzuki, T.; Miyashi, T.; Yamashita, Y. Single-component organic conductors based on neutral radicals containing the pyrazino-TCNQ skeleton. *J. Org. Chem.* **1992**, *57* (25), 6749-6755.
(119) Zibarev, A. V.; Miller, A. O. Cyclic aryleneazachalcogenenes. Part III [1] synthesis of polyfluorinated 2,1,3-benzothia-(selena) diazoles. *J. Fluorine Chem.* **1990**, *50* (3), 359-363.
(120) Carvalho, T. O.; Carvalho, P.; Correa, J. R.; Guido, B. C.; Medeiros, G. A.; Eberlin, M. N.; Coelho, S. E.; Domingos, J. B.; Neto, B. A. D. Palladium Catalyst with Task-Specific Ionic Liquid Ligands: Intracellular Reactions and Mitochondrial Imaging with Benzothiadiazole Derivatives. *J. Org. Chem.* **2019**, *84* (9), 5118-5128.
(121) Medeiros, G. A.; Correa, J. R.; de Andrade, L. P.; Lopes, T. O.; de Oliveira, H. C. B.; Diniz, A. B.; Menezes, G. B.; Rodrigues, M. O.; Neto, B. A. D. A benzothiadiazole-quinoline hybrid sensor for specific bioimaging and surgery procedures in mice. *Sens. Actuators, B* **2021**, *328*, 128998.
(122) Carvalho, P. H. P. R.; Correa, J. R.; Paiva, K. L. R.; Baril, M.; Machado, D. F. S.; Scholten, J. D.; de Souza, P. E. N.; Veiga-Souza, F. H.; Spencer, J.; Neto, B. A. D. When the strategies for cellular selectivity fail. Challenges and surprises in the design and application of fluorescent benzothiadiazole derivatives for mitochondrial staining. *Org. Chem. Front.* **2019**, *6* (14), 2371-2384.
(123) Han, X.; Wang, Z.; Cheng, Q.; Meng, X.; Wei, D.; Zheng, Y.; Ding, J.; Hou, H. Mitochondria-dependent benzothiadiazole-based molecule probe for quantitatively intracellular pH imaging. *Dyes Pigm.* **2017**, *145*, 576-583.
(124) Neto, B. A. D.; Carvalho, P. H. P. R.; Santos, D. C. B. D.; Gatto, C. C.; Ramos, L. M.; Vasconcelos, N. M. d.; Corrêa, J. R.; Costa, M. B.; de Oliveira, H. C. B.; Silva, R. G. Synthesis, properties and highly selective mitochondria staining with novel, stable and superior benzothiadiazole fluorescent probes. *RSC Adv.* **2012**, *2* (4), 1524-1532.
(125) Sodre, E. R.; Guido, B. C.; de Souza, P. E. N.; Machado, D. F. S.; Carvalho-Silva, V. H.; Chaker, J. A.; Gatto, C. C.; Correa, J. R.; Fernandes, T. A.; Neto, B. A. D. Deciphering the Dynamics of Organic Nanoaggregates with AIEE Effect and Excited States: Lipophilic Benzothiadiazole Derivatives as Selective Cell Imaging Probes. *J. Org. Chem.* **2020**, *85* (19), 12614-12634.
(126) Appelqvist, H.; Stranius, K.; Börjesson, K.; Nilsson, K. P. R.; Dyrager, C. Specific Imaging of Intracellular Lipid Droplets Using a Benzothiadiazole Derivative with Solvatochromic Properties. *Bioconjugate Chem.* **2017**, *28* (5), 1363-1370.
(127) Reichardt, C. Solvatochromic Dyes as Solvent Polarity Indicators. *Chem. Rev.* **1994**, *94* (8), 2319-2358.
(128) Maillard, J.; Klehs, K.; Rumble, C.; Vauthey, E.; Heilemann, M.; Fürstenberg, A. Universal quenching of common fluorescent probes by water and alcohols. *Chem. Sci.* **2021**, *12* (4), 1352-1362.

(129) Minesinger, R. R.; Kayser, E. G.; Kamlet, M. J. Solvatochromic shifts for some 4-nitroani- line and 4-nitrophenol derivatives as measures of relative solvent proton affinities. *J. Org. Chem.* **1971**, *36* (10), 1342-1345.
(130) Suppan, P. Solvatochromic shifts: The influence of the medium on the energy of electronic states. *J. Photochem. Photobiol. A* **1990**, *50* (3), 293-330.
(131) Li, W.; Wang, L.; Tang, H.; Cao, D. An interface-targeting and H2O2-activatable probe liberating AIEgen: enabling on-site imaging and dynamic movement tracking of lipid droplets. *Chem. Commun.* **2019**, *55* (31), 4491-4494.
(132) Shi, X.; Sung, S. H. P.; Lee, M. M. S.; Kwok, R. T. K.; Sung, H. H. Y.; Liu, H.; Lam, J. W. Y.; Williams, I. D.; Liu, B.; Tang, B. Z. A lipophilic AIEgen for lipid droplet imaging and evaluation of the efficacy of HIF-1 targeting drugs. *J. Mater. Chem. B* **2020**, *8* (7), 1516-1523.
(133) Xu, Y.; Zhang, H.; Zhang, N.; Xu, R.; Wang, Z.; Zhou, Y.; Shen, Q.; Dang, D.; Meng, L.; Tang, B. Z. An easily synthesized AIE luminogen for lipid droplet-specific super-resolution imaging and two-photon imaging. *Mater. Chem. Front.* **2021**, *5* (4), 1872-1883.
(134) Yu, Y.; Xing, H.; Park, H.; Zhang, R.; Peng, C.; Sung, H. H. Y.; Williams, I. D.; Ma, C.; Wong, K. S.; Li, S.; Xiong, Q.; Li, M.-H.; Zhao, Z.; Tang, B. Z. Deep-Red Aggregation-Induced Emission Luminogen Based on Dithiofuvalene-Fused Benzothiadiazole for Lipid Droplet-Specific Imaging. *ACS Materials Lett.* **2022**, *4* (1), 159-164.
(135) Fujimoto, Y.; Onoduka, J.; Homma, K. J.; Yamaguchi, S.; Mori, M.; Higashi, Y.; Makita, M.; Kinoshita, T.; Noda, J.-i.; Itabe, H.; Takanoa, T. Long-Chain Fatty Acids Induce Lipid Droplet Formation in a Cultured Human Hepatocyte in a Manner Dependent of Acyl-CoA Synthetase. *Biol. Pharm. Bull.* **2006**, *29* (11), 2174-2180.
(136) Rohwedder, A.; Zhang, Q.; Rudge, S. A.; Wakelam, M. J. O. Lipid droplet formation in response to oleic acid in Huh-7 cells is mediated by the fatty acid receptor FFAR4. *J. Cell Sci.* **2014**, *127* (14), 3104-3115.
(137) Nakajima, S.; Gotoh, M.; Fukasawa, K.; Murakami-Murofushi, K.; Kunugi, H. Oleic acid is a potent inducer for lipid droplet accumulation through its esterification to glycerol by diacylglycerol acyltransferase in primary cortical astrocytes. *Brain Res.* **2019**, *1725*, 146484.
(138) Präbst, K.; Engelhardt, H.; Ringgeler, S.; Hübner, H. Basic Colorimetric Proliferation Assays: MTT, WST, and Resazurin. In *Cell Viability Assays: Methods and Protocols*, Gilbert, D. F., Friedrich, O. Eds.; Springer New York, 2017; pp 1-17.
(139) Molinspiration Cheminformatics free web services. https://molinspiration.com/ (accessed 24 July 2023).
(140) Horobin, R. W.; Rashid-Doubell, F.; Pediani, J. D.; Milligan, G. Predicting small molecule fluorescent probe localization in living cells using QSAR modeling. 1. Overview and models for probes of structure, properties and function in single cells. *Biotech. Histochem.* **2013**, *88* (8), 440-460.
(141) Niu, G.; Zhang, R.; Kwong, J. P. C.; Lam, J. W. Y.; Chen, C.; Wang, J.; Chen, Y.; Feng, X.; Kwok, R. T. K.; Sung, H. H. Y.; Williams, I. D.; Elsegood, M. R. J.; Qu, J.; Ma, C.; Wong, K. S.; Yu, X.; Tang, B. Z. Specific Two-Photon Imaging of Live Cellular and Deep-Tissue Lipid Droplets by Lipophilic AIEgens at Ultralow Concentration. *Chem. Mater.* **2018**, *30* (14), 4778-4787.
(142) Suarez, S. I.; Warner, C. C.; Brown-Harding, H.; Thooft, A. M.; VanVeller, B.; Lukesh, J. C. Highly selective staining and quantification of intracellular lipid droplets with a compact push-pull fluorophore based on benzothiadiazole. *Org. Biomol. Chem.* **2020**, *18* (3), 495-499.

(143) Wu, X.; Guo, Z.; Wu, Y.; Zhu, S.; James, T. D.; Zhu, W. Near-Infrared Colorimetric and Fluorescent Cu2+ Sensors Based on Indoline–Benzothiadiazole Derivatives via Formation of Radical Cations. *ACS Appl. Mater. Interfaces* **2013**, *5* (22), 12215-12220.
(144) Nishimura, Y.; Yata, K.; Nomoto, T.; Ogiwara, T.; Watanabe, K.; Shintou, T.; Tsuboyama, A.; Okano, M.; Umemoto, N.; Zhang, Z.; Kawabata, M.; Zhang, B.; Kuroyanagi, J.; Shimada, Y.; Miyazaki, T.; Imamura, T.; Tomimoto, H.; Tanaka, T. Identification of a Novel Indoline Derivative for in Vivo Fluorescent Imaging of Blood-Brain Barrier Disruption in Animal Models. *ACS Chem. Neurosci.* **2013**, *4* (8), 1183-1193.
(145) Splitstoser, J. C.; Dillehay, T. D.; Wouters, J.; Claro, A. Early pre-Hispanic use of indigo blue in Peru. *Sci. Adv.* **2016**, *2* (9), e1501623.
(146) Petermayer, C.; Dube, H. Indigoid Photoswitches: Visible Light Responsive Molecular Tools. *Acc. Chem. Res.* **2018**, *51* (5), 1153-1163.
(147) Lee, J. H.; So, J.-H.; Jeon, J. H.; Choi, E. B.; Lee, Y.-R.; Chang, Y.-T.; Kim, C.-H.; Bae, M. A.; Ahn, J. H. Synthesis of a new fluorescent small molecule probe and its use for in vivolipid imaging. *Chem. Commun.* **2011**, *47* (26), 7500-7502.
(148) Chun, H.-S.; Jeon, J. H.; Pagire, H. S.; Lee, J. H.; Chung, H.-C.; Park, M. J.; So, J.-H.; Ryu, J.-H.; Kim, C.-H.; Ahn, J. H.; Bae, M. A. Synthesis of LipidGreen2 and its application in lipid and fatty liver imaging. *Mol. Biosyst.* **2013**, *9* (4), 630-633.
(149) Chen, H.; Shang, H.; Liu, Y.; Guo, R.; Lin, W. Development of a Unique Class of Spiro-Type Two-Photon Functional Fluorescent Dyes and Their Applications for Sensing and Bioimaging. *Adv. Funct. Mater.* **2016**, *26* (44), 8128-8136.
(150) Pal, K.; Koner, A. L. Rationally Designed Solvatochromic Fluorescent Indoline Derivatives for Probing Mitochondrial Environment. *Chem. Eur. J.* **2017**, *23* (36), 8610-8614.
(151) Pal, K.; Sharma, A.; Koner, A. L. Synthesis of Two-Photon Active Tricomponent Fluorescent Probe for Distinguishment of Biotin Receptor Positive and Negative Cells and Imaging 3D-Spheroid. *Org. Lett.* **2018**, *20* (20), 6425-6429.
(152) Pal, K.; Kumar, P.; Koner, A. L. Deciphering interior polarity of lysosome in live cancer and normal cells using spectral scanning microscopy. *J. Photochem. Photobiol., B* **2020**, *206*, 111848.
(153) Kam, T.-S.; Subramaniam, G.; Lim, K.-H.; Choo, Y.-M. Mersicarpine, an unusual tetracyclic dihydroindole alkaloid incorporating a seven-membered imine ring. *Tetrahedron Lett.* **2004**, *45* (31), 5995-5998.
(154) Tan, C.-J.; Di, Y.-T.; Wang, Y.-H.; Zhang, Y.; Si, Y.-K.; Zhang, Q.; Gao, S.; Hu, X.-J.; Fang, X.; Li, S.-F.; Hao, X.-J. Three New Indole Alkaloids from Trigonostemon lii. *Org. Lett.* **2010**, *12* (10), 2370-2373.
(155) Leijendekker, L. H.; Weweler, J.; Leuther, T. M.; Streuff, J. Catalytic Reductive Synthesis and Direct Derivatization of Unprotected Aminoindoles, Aminopyrroles, and Iminoindolines. *Angew. Chem. Int. Ed.* **2017**, *56* (22), 6103-6106.
(156) Leijendekker, L. H.; Weweler, J.; Leuther, T. M.; Kratzert, D.; Streuff, J. Development, Scope, and Applications of Titanium(III)-Catalyzed Cyclizations to Aminated N-Heterocycles. *Chem. Eur. J.* **2019**, *25* (13), 3382-3390.

(157) Sulsky, R.; Gougoutas, J. Z.; DiMarco, J.; Biller, S. A. Conformational Switching and the Synthesis of Spiro[2H-indol]-3(1H)-ones by Radical Cyclization. *J. Org. Chem.* **1999**, *64* (15), 5504-5510.
(158) Boger, D. L.; McKie, J. A.; Nishi, T.; Ogiku, T. Enantioselective Total Synthesis of (+)-Duocarmycin A, epi-(+)-Duocarmycin A, and Their Unnatural Enantiomers. *J. Am. Chem. Soc.* **1996**, *118* (9), 2301-2302.
(159) Xu, Z.; Wang, X.-G.; Wei, Y.-H.; Ji, K.-L.; Zheng, J.-F.; Ye, J.-L.; Huang, P.-Q. Organocatalytic, Enantioselective Reductive Bis-functionalization of Secondary Amides: One-Pot Construction of Chiral 2,2-Disubstituted 3-Iminoindoline. *Org. Lett.* **2019**, *21* (18), 7587-7591.
(160) Culbertson, J. B. Factors Affecting the Rate of Hydrolysis of Ketimines. *J. Am. Chem. Soc.* **1951**, *73* (10), 4818-4823.
(161) Chrystiuk, E.; Williams, A. A single transition-state in the transfer of the methoxycarbonyl group between isoquinoline and substituted pyridines in aqueous solution. *J. Am. Chem. Soc.* **1987**, *109* (10), 3040-3046.
(162) Ireland, J. F.; Wyatt, P. A. H. Acid-Base Properties of Electronically Excited States of Organic Molecules. *Adv. Phys. Org. Chem.* **1976**, *12*, 131-221.
(163) Arnaut, L. G.; Formosinho, S. J. Excited-state proton transfer reactions I. Fundamentals and intermolecular reactions. *J. Photochem. Photobiol. A* **1993**, *75* (1), 1-20.
(164) Tolbert, L. M.; Solntsev, K. M. Excited-State Proton Transfer: From Constrained Systems to "Super" Photoacids to Superfast Proton Transfer. *Acc. Chem. Res.* **2002**, *35* (1), 19-27.
(165) Agmon, N. Elementary Steps in Excited-State Proton Transfer. *J. Phys. Chem. A* **2005**, *109* (1), 13-35.
(166) Hunt, J. R.; Tseng, C.; Dawlaty, J. M. Donor–acceptor preassociation, excited state solvation threshold, and optical energy cost as challenges in chemical applications of photobases. *Faraday Discuss.* **2019**, *216*, 252-268.
(167) Marciniak, B.; Kozubek, H.; Paszyc, S. Estimation of pKa* in the first excited singlet state. A physical chemistry experiment that explores acid-base properties in the excited state. *J. Chem. Educ.* **1992**, *69* (3), 247-249.
(168) Sheng, W.; Nairat, M.; Pawlaczyk, P. D.; Mroczka, E.; Farris, B.; Pines, E.; Geiger, J. H.; Borhan, B.; Dantus, M. Ultrafast Dynamics of a "Super" Photobase. *Angew. Chem. Int. Ed.* **2018**, *57* (45), 14742-14746.
(169) Jiménez-Sánchez, A.; Santillan, R. A photochromic–acidochromic HCl fluorescent probe. An unexpected chloride-directed recognition. *Analyst* **2016**, *141* (13), 4108-4120.
(170) Driscoll, E. W.; Hunt, J. R.; Dawlaty, J. M. Photobasicity in Quinolines: Origin and Tunability via the Substituents' Hammett Parameters. *J. Phys. Chem. Lett.* **2016**, *7* (11), 2093-2099.
(171) Ballinger, P.; Long, F. A. Acid Ionization Constants of Alcohols. II. Acidities of Some Substituted Methanols and Related Compounds1,2. *J. Am. Chem. Soc.* **1960**, *82* (4), 795-798.
(172) Hunt, J. R.; Dawlaty, J. M. Photodriven Deprotonation of Alcohols by a Quinoline Photobase. *J. Phys. Chem. A* **2018**, *122* (40), 7931-7940.
(173) Kingerley, R. W.; LaMer, V. K. Exchange and Transfer Equilibria of Acids, Bases, and Salts in Deuterium-Protium Oxide Mixtures. The Ion Product Constant of Deuterium Oxide. *J. Am. Chem. Soc.* **1941**, *63* (12), 3256-3262.
(174) Gold, V.; Grist, S. Deuterium solvent isotope effects in methanol solution. Part I. Fractionation factors for lyonium and lyate ions. *J. Chem. Soc. B* **1971**, 1665-1670.

(175) Webb, B. A.; Chimenti, M.; Jacobson, M. P.; Barber, D. L. Dysregulated pH: a perfect storm for cancer progression. *Nat. Rev. Cancer* **2011**, *11* (9), 671-677.
(176) Webb, B. A.; Aloisio, F. M.; Charafeddine, R. A.; Cook, J.; Wittmann, T.; Barber, D. L. pHLARE: a new biosensor reveals decreased lysosome pH in cancer cells. *Mol. Biol. Cell* **2021**, *32* (2), 131-142.
(177) Hall, H. K., Jr. Potentiometric Determination of the Base Strength of Amines in Non-protolytic Solvents. *J. Phys. Chem.* **1956**, *60* (1), 63-70.
(178) Settembre, C.; Fraldi, A.; Medina, D. L.; Ballabio, A. Signals from the lysosome: a control centre for cellular clearance and energy metabolism. *Nat. Rev. Mol. Cell Biol.* **2013**, *14* (5), 283-296.
(179) El-Sayed, M. A. Triplet state. Its radiative and nonradiative properties. *Acc. Chem. Res.* **1968**, *1* (1), 8-16.
(180) Marian, C. M. Understanding and Controlling Intersystem Crossing in Molecules. *Annu. Rev. Phys. Chem.* **2021**, *72* (1), 617-640.
(181) Nikolov, P.; Petkova, I.; Köhler, G.; Stojanov, S. Deactivation processes and hydrogen bonding of excited N-substituted acridones. *J. Mol. Struct.* **1998**, *448* (2), 247-254.
(182) Gomes, A.; Fernandes, E.; Lima, J. L. F. C. Fluorescence probes used for detection of reactive oxygen species. *J. Biochem. Biophys. Methods* **2005**, *65* (2), 45-80.
(183) Litwinienko, G.; Ingold, K. U. Solvent Effects on the Rates and Mechanisms of Reaction of Phenols with Free Radicals. *Acc. Chem. Res.* **2007**, *40* (3), 222-230.
(184) Litwinienko, G.; Beckwith, A. L. J.; Ingold, K. U. The frequently overlooked importance of solvent in free radical syntheses. *Chem. Soc. Rev.* **2011**, *40* (5), 2157-2163.
(185) Robinson-Duggon, J.; Mariño-Ocampo, N.; Barrias, P.; Zúñiga-Núñez, D.; Günther, G.; Edwards, A. M.; Greer, A.; Fuentealba, D. Mechanism of Visible-Light Photooxidative Demethylation of Toluidine Blue O. *J. Phys. Chem. A* **2019**, *123* (23), 4863-4872.
(186) Pratt, A. C. The photochemistry of imines. *Chem. Soc. Rev.* **1977**, *6* (1), 63-81.
(187) Uraguchi, D.; Tsuchiya, Y.; Ohtani, T.; Enomoto, T.; Masaoka, S.; Yokogawa, D.; Ooi, T. Unveiling Latent Photoreactivity of Imines. *Angew. Chem. Int. Ed.* **2020**, *59* (9), 3665-3670.
(188) Kettner, A.; Griehl, C. The use of LipidGreen2 for visualization and quantification of intracellular Poly(3-hydroxybutyrate) in Cupriavidus necator. *Biochem. Biophys. Rep.* **2020**, *24*, 100819.
(189) Waldeck, D. H. Photoisomerization dynamics of stilbenes. *Chem. Rev.* **1991**, *91* (3), 415-436.
(190) Bandara, H. M. D.; Burdette, S. C. Photoisomerization in different classes of azobenzene. *Chem. Soc. Rev.* **2012**, *41* (5), 1809-1825.
(191) Irie, M.; Fukaminato, T.; Matsuda, K.; Kobatake, S. Photochromism of Diarylethene Molecules and Crystals: Memories, Switches, and Actuators. *Chem. Rev.* **2014**, *114* (24), 12174-12277.
(192) Klajn, R. Spiropyran-based dynamic materials. *Chem. Soc. Rev.* **2014**, *43* (1), 148-184.
(193) Berkovic, G.; Krongauz, V.; Weiss, V. Spiropyrans and Spirooxazines for Memories and Switches. *Chem. Rev.* **2000**, *100* (5), 1741-1754.
(194) Minkin, V. I. Photo-, Thermo-, Solvato-, and Electrochromic Spiroheterocyclic Compounds. *Chem. Rev.* **2004**, *104* (5), 2751-2776.

(195) Yokoyama, Y. Fulgides for Memories and Switches. *Chem. Rev.* **2000**, *100* (5), 1717-1740.
(196) Lachmann, D.; Lahmy, R.; König, B. Fulgimides as Light-Activated Tools in Biological Investigations. *Eur. J. Org. Chem.* **2019**, *2019* (31-32), 5018-5024.

# 9 Appendix

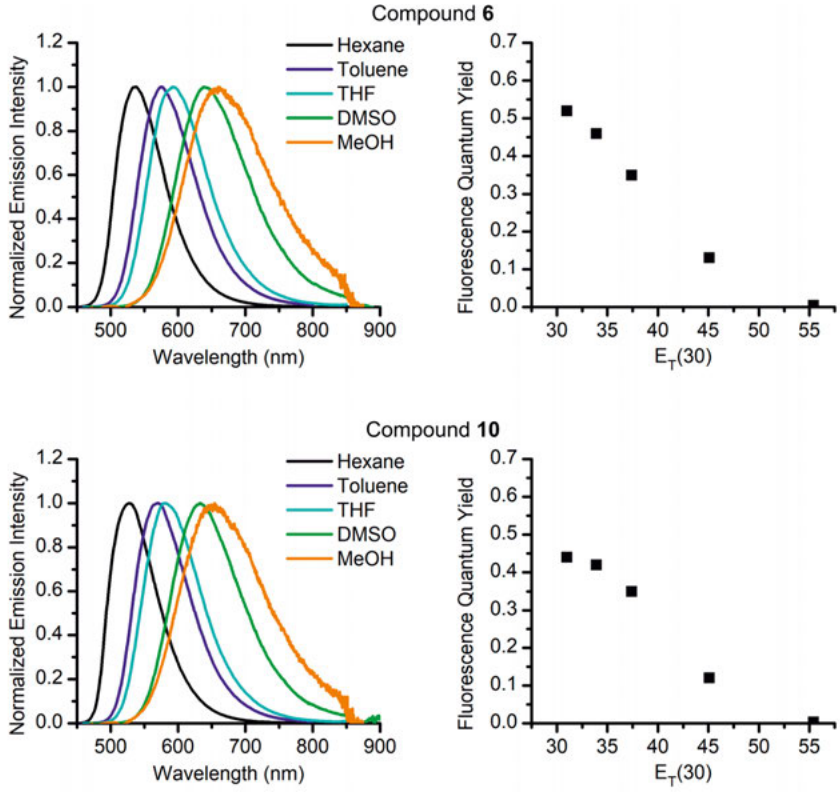


Figure A1. Remeasured normalized emission spectra of piperidino-BTD **6** and pyrrolidino-BTD **10** in various solvents, showing positive solvatochromism. Correlations between the remeasured fluorescence quantum yields and the $E_T(30)$ solvent polarity parameter (in kcal/mol) are shown on the right.

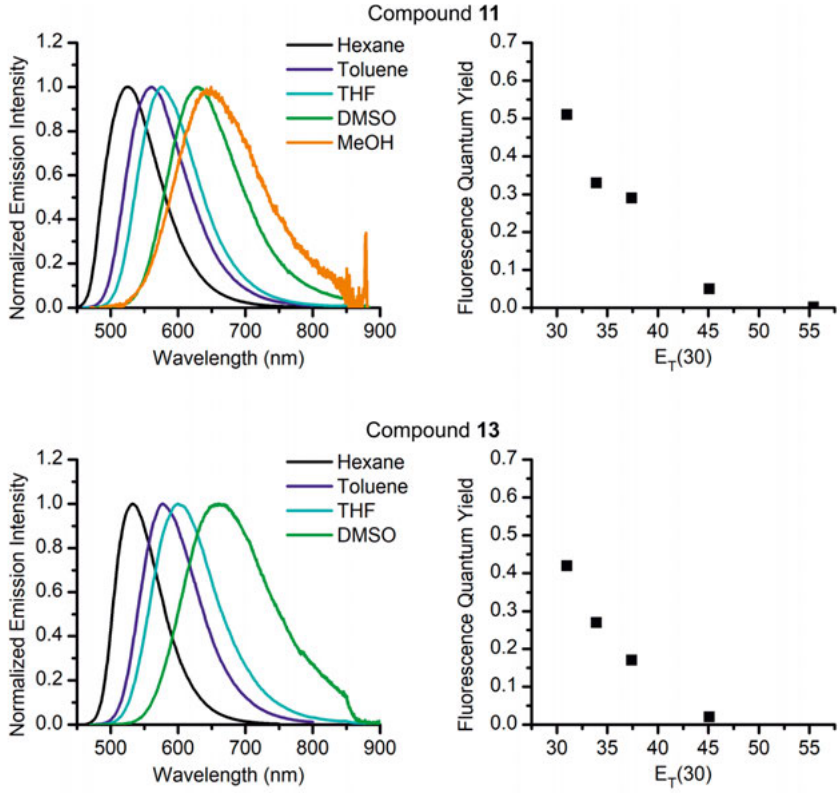


Figure A2. Remeasured normalized emission spectra of cyclohexylamino-BTD **11** and diphenylamino-BTD **13** in various solvents, showing positive solvatochromism. Correlations between the remeasured fluorescence quantum yields and the $E_T(30)$ solvent polarity parameter (in kcal/mol) are shown on the right.

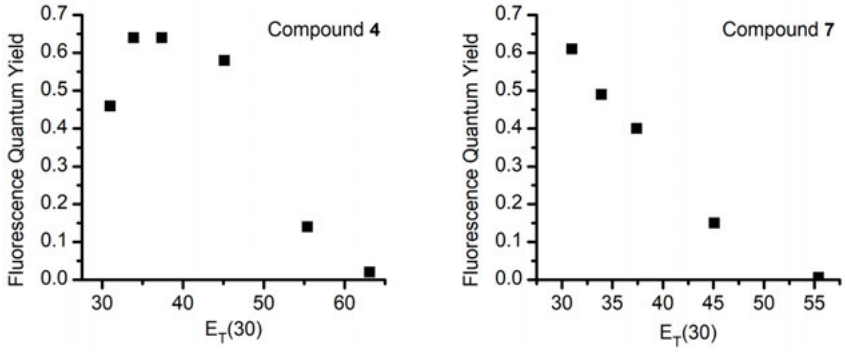


Figure A3. Correlations between the remeasured fluorescence quantum yields of amido-BTD **4** or morpholino-BTD **7** and the $E_T(30)$ solvent polarity parameter (in kcal/mol).

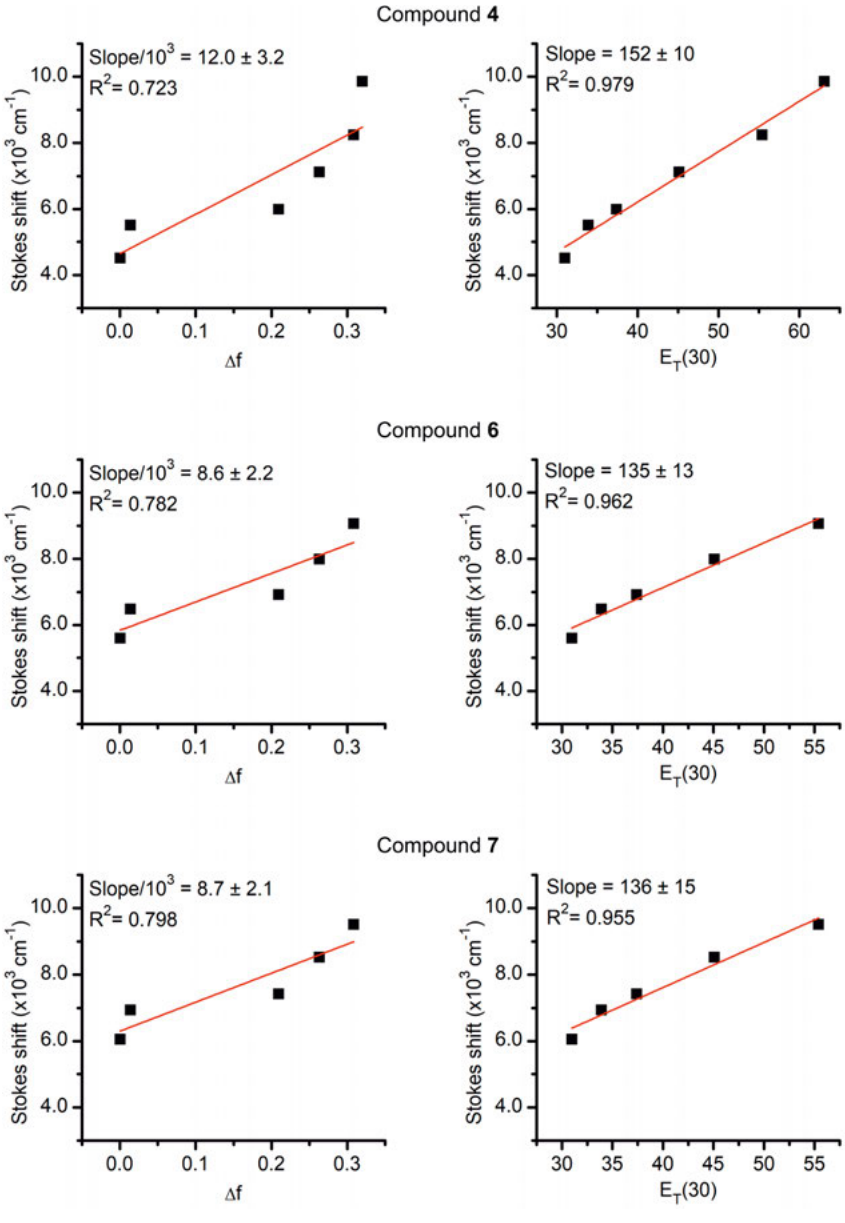


Figure A4. Correlation between Stokes shifts (based on remeasured $\lambda_{Emax}$) and the orientation polarizability parameter ($\Delta f$) of the solvents (i.e., the Lippert-Mataga plot; left) or the $E_T(30)$ solvent polarity parameter (in kcal/mol; right) for compounds **4**, **6**, and **7**. The plots against $E_T(30)$ show better linearity.

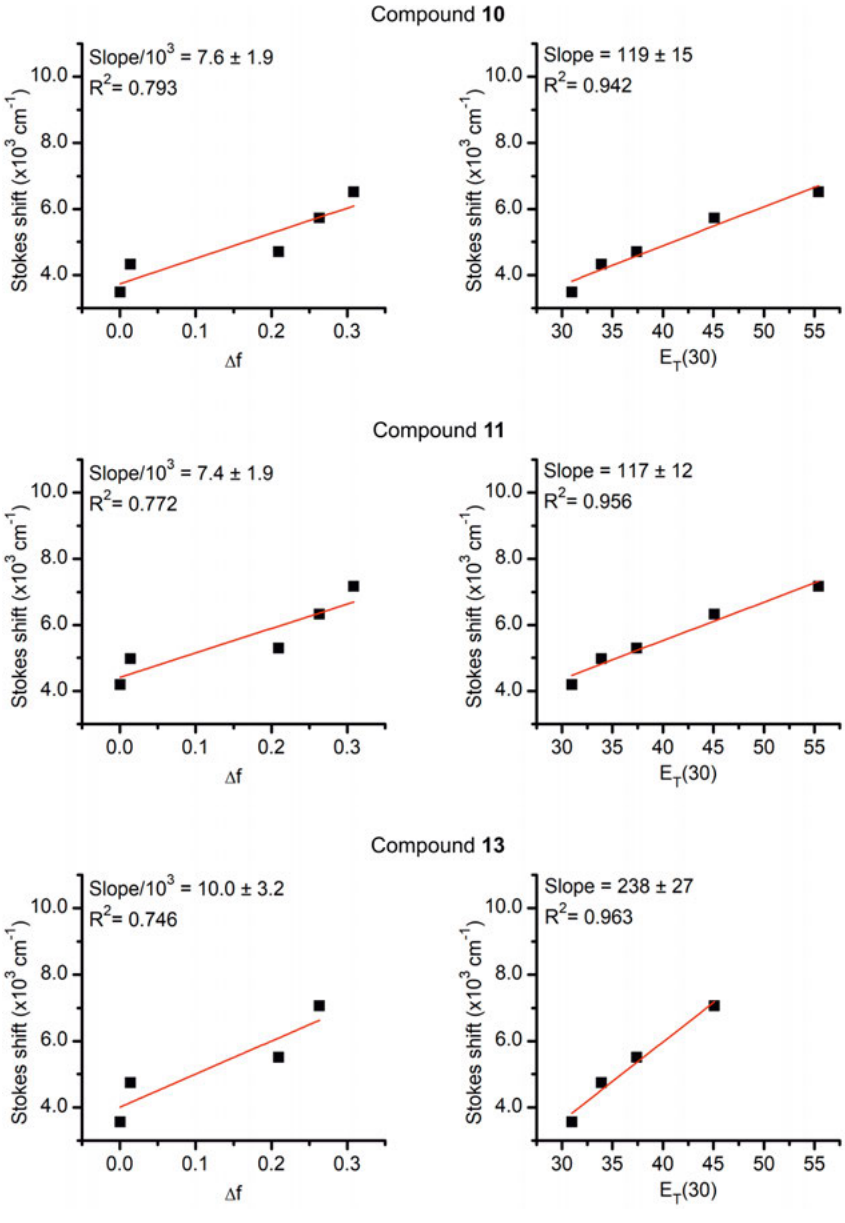


Figure A5. Correlation between Stokes shifts (based on remeasured $\lambda_{Emax}$) and the orientation polarizability parameter ($\Delta f$) of the solvents (i.e., the Lippert-Mataga plot; left) or the $E_T(30)$ solvent polarity parameter (in kcal/mol; right) for compounds **10**, **11**, and **13**. The plots against $E_T(30)$ show better linearity.

Acta Universitatis Upsaliensis

*Digital Comprehensive Summaries of Uppsala Dissertations from the Faculty of Science and Technology* 2291

Editor: The Dean of the Faculty of Science and Technology

A doctoral dissertation from the Faculty of Science and Technology, Uppsala University, is usually a summary of a number of papers. A few copies of the complete dissertation are kept at major Swedish research libraries, while the summary alone is distributed internationally through the series Digital Comprehensive Summaries of Uppsala Dissertations from the Faculty of Science and Technology. (Prior to January, 2005, the series was published under the title "Comprehensive Summaries of Uppsala Dissertations from the Faculty of Science and Technology".)

Distribution: publications.uu.se
urn:nbn:se:uu:diva-508762

ACTA UNIVERSITATIS
UPSALIENSIS
2023